2009

Multifunctional Nanocomposites For High Damping Performance

Lee Algozzini
University of Central Florida

MULTIFUNCTIONAL NANOCOMPOSITES FOR HIGH DAMPING PERFORMANCE

by

LEE DOUGLAS ALGOZZINI
B.S. University of Central Florida, 2007

A thesis submitted in partial fulfillment of the requirements
for the degree of Master of Science
in the Department of Mechanical, Materials, and Aerospace Engineering
in the College of Engineering and Computer Sciences
at the University of Central Florida
Orlando, Florida

Summer Term
2009

ABSTRACT

Composite structures for aerospace and wind turbine applications are subjected to high acoustic and vibrational loading and exhibit very high amplitude displacements and thus premature failure. Materials with high damping or absorbing properties are crucially important to extend the life of structures. Traditional damping treatments are based on the combinations of viscoelastic, elastomeric, magnetic, and piezoelectric materials.

In this work, the use of carbon nanofibers (CNFs) in the form of interconnected self-supportive paper as reinforcement can significantly improve damping performance. The interfacial friction is the primary source of energy dissipation in CNF paper based nanocomposites. The approach entailed making CNF paper by filtration of well-dispersed nanofibers under controlled processing conditions. The CNF paper was integrated into composite laminates using modified liquid composite molding processes including Resin Transfer Molding (RTM) and Vacuum Assisted Resin Transfer Molding (VARTM).

The rheological and curing behaviors of the CNF-modified polymer resin were characterized with Viscometry and Differential Scanning Calorimetry (DSC). The process analysis in mold filling and pressure distribution was conducted using Control Volume Finite Element Method (CVFEM) in an attempt to optimize the quality of multifunctional nanocomposites. The mold filling simulation was validated with flow visualization in a transparent mold. Several tests were performed to study the damping properties of the fabricated composites including Dynamic Mechanical Analysis (DMA) and piezoceramic patch based vibration tests. It was found that the damping performance was significantly enhanced with the incorporation of carbon nanofibers into the composite structures.

I dedicate this thesis to my parents, especially my mom.

Without both of their patience, understanding, support, and most of all love,

the completion of this work would not have been possible.

ACKNOWLEDGMENTS

I would first like to thank my research director, Dr. Jan Gou, for introducing me to the world of nanocomposites. His teaching and guidance have amounted to an invaluable learning experience for me over the past couple of years. He is an outstanding model of success in an emergent and tremendously beneficial field.

I would also like to thank Dr. Zhongfu Zhao and Dr. Yong Tang for being exceptional laboratory instructors, and for being such vast fountains of knowledge in their respective fields. They have bestowed upon me a great wealth of knowledge of compositing techniques.

Special recognition also needs to be given to my colleagues for their continued support of my research and never-ending eagerness to lend a hand. Thank you Fei Liang, Jinfeng Zhuge, and Haibao Lu. I am grateful for all of your contributions to my work. Appreciation must also be shown to Marvin Tsoi and Yan Hong for assisting me with experiments that I could not have completed on my own. Thank you Ricky McKee for being a first-rate laboratory manager, and all-around idea guy. Last, but not least, thanks to Jeremy Lawrence and Richie Bertrand for their innovative design and fabrication of a composite mold essential to the success of this research.

Thank you all so much!

TABLE OF CONTENTS

LIST OF FIGURES

LIST OF TABLES

CHAPTER 1.

INTRODUCTION

Composite structures for aerospace and wind turbine applications are subjected to high acoustic and vibrational loading and exhibit very high amplitude displacements and thus premature failure. Materials with high damping or absorbing properties are crucially important to extend the life of structures. The vibration and acoustic reduction can be obtained in structural materials by increasing the damping capacity (expressed by the loss factor) and/or decreasing the stiffness (expressed by the storage modulus). Traditional damping polymers perform poorly at elevated temperatures. Nanocomposites can provide excellent damping at high temperatures, suggesting a great potential for a variety of applications in aircraft, spacecraft, satellites, automobiles, wind turbines, sensors for missile systems, as well as any structure that is exposed to unwanted vibrations (Guo et al, 2006). Established damping treatments are based on the combinations of viscoelastic, elastomeric, magnetic, and piezoelectric materials.

The objective of this research is to develop optimal processes for production of nanocomposites for high vibrational or acoustic damping applications. The methodology behind this essentially consists of the introduction of nano-scale particles into traditional composite laminates for the purpose of increasing their damping characteristics. The interfacial friction between each of the nanoparticles is the primary source of energy dissipation in CNF paper based nanocomposites. In CNF-modified polymer composites, the interfacial friction between the nanoparticles and the polymer resin are also a main source of energy dissipation (Suhr, 2008). This has been found to be the dominant damping mechanism between the two. This damping mechanism is illustrated in Figure 1.

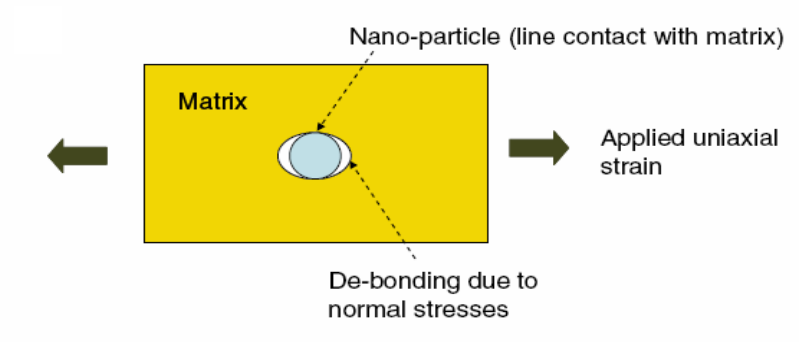

Figure 1: Illustration of the damping mechanism within nanocomposites

As a uniaxial strain is applied to the matrix of the nanocomposite, the nanoparticles de-bond from the matrix in the applied direction. In response to this, the particle remains in contact with the matrix in the transverse direction, while sliding out of plane in the third direction. The friction generated from this interfacial sliding is the primary source of energy dissipation. This interfacial slip between the surface of the nanoparticle and matrix result in very high mechanical damping. The same is true in CNF paper based nanocomposites, where the nanoparticles are in contact with other nanoparticles in stead of a polymer matrix. The aspect ratio of the nanoparticles greatly contributes to their damping properties. With a higher aspect ratio, comes increased interfacial contact. For this reason, nanofibers are used rather than shorter nanofillers.

Other advantages of carbon nanofibers include high elastic modulus, high tensile modulus, low density, and seamless integration into composite systems without sacrificing structural integrity or mechanical strength. The carbon nanofibers utilized in this research have diameters ranging from 50 to 200 nm, and lengths ranging from 30 to 100 nm. Their tensile strength and modulus ranged from 400 to 600 GPa and 2.7 to 7.0 GPa respectively.

In this research, carbon nanofibers (CNFs) were introduced into traditional composite laminates in one of two distinct methods. The first technique involved dispersing the CNFs into the polymer resin, followed by infusing the carbon fiber preform sheets with this CNF-modified resin. The second method entailed adding a single layer of CNF paper to the fiber sheets, and subsequently infusing the fiber layers and CNF paper with a polymer resin. Both methods were completed by curing the fiber and resin in a closed mold at high temperatures.

The CNF paper-making process consists of three essential steps. The carbon nanofibers are initially pre-mixed in an aqueous solution. That solution is sonicated in an ultra-sonication device, which uniformly disperses the nanofibers throughout the solution. Proper dispersion of nanofibers is vital to producing high quality CNF paper. The sonicated solution is then filtered using a polycarbonate membrane to form a single layer of CNF paper. The paper can be manufactured thinner than 0.5 mm. The CNF paper manufacturing process is illustrated in Figure 2. In Figure 3, a single layer of CNF paper displays good strength and flexibility to allow for handling like traditional fiber mats.

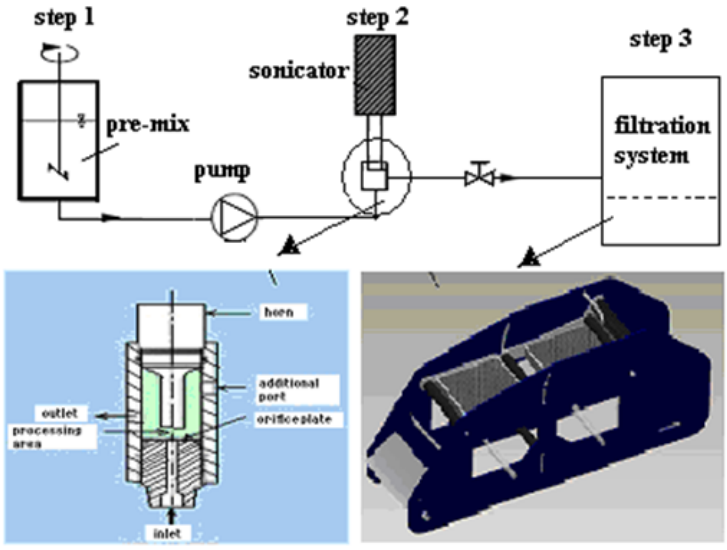

Figure 2: Illustration of CNF paper manufacturing

Figure 3: Carbon nanofiber paper

This research study focuses on examining the manufacturing processes and resulting damping performance of carbon fiber reinforced polymer resin containing various amounts of carbon nanofiber particles. This includes rheologically testing epoxy resin containing various amounts of carbon nanofibers, flow analysis on identical resin, and mechanically testing various nanocomposite samples containing either CNF paper or CNF-modified epoxy. The rheological analysis includes Viscometry and Differential Scanning Calorimetry. The flow analysis includes a computational simulation using Control Volume Finite Element Method (CVFEM), as well as physical visualization. The damping analysis includes Dynamic Mechanical Analysis (DMA) and piezoceramic patch-based vibration tests.

It is believed that the damping performance is enhanced by the incorporation of carbon nanofibers into composite structures. Nanocomposites developed for their vibrational and acoustic damping characteristics require a balance of proper design and precise processing. Appropriate types and amounts of reinforcing fibers, polymer resins, nanoparticles, injection processes, curing temperatures, and curing times are necessary to produce a successful product.

CHAPTER 2.

LITERATURE REVIEW

2.1 Fiber-Reinforced Epoxy Resins

Composites are usually called reinforced plastics. They are composed of a continuous reinforcing fiber and a polymer matrix. Thermoset resins, such as epoxy resins, have high heat resistance and great structural durability. While reinforcing fibers can provide strength and stiffness, epoxy resin can give the desired shape or structure to a composite and distribute the stress between the enforced fibers. The combination of high strength of the reinforcing fiber and the epoxy matrix gives composites many desirable chemical and physical properties. They have high strength and can meet specific strength requirements in engineering applications. They have high stiffness and meet the low deformation requirement under high load. Compared to steel and aluminum, they have the highest ratio of strength to weight, which is one of the important requirements in the aerospace industry. Chemically, they are stable and have excellent resistance against corrosion and wearing. Economically, they are cost-effective materials and easy to use.

Because of these unique chemical and physical properties, the fiber-reinforced epoxy composites find applications in many areas such as spacecraft, aircraft, marine vessels, corrosion-resistant chemical tanks, electrical equipment, automotive vehicles, reinforced epoxy pipes, and other construction materials. Many composite products are manufactured from different prepregs. Several factors such as epoxy resin, curing agent, reinforcing fiber, fiber orientation, and volume fraction of fibers significantly affect the properties of the overall composite.

2.2 Damping Properties

The damping property of a material signifies its ability to reduce the transmission of vibration caused by mechanical disturbances. The measure of damping for a material is its damping factor η. A high value of η is desirable for reducing the amplitude of vibration in a structure. Table 1 compares typical damping factors for various polymer laminates to steel and aluminum. Fiber-reinforced composites, in general, have a higher damping factor than metals (Mallick, 2008). However, its value depends on a number of factors, including fiber and resin types, fiber orientation angle, and stacking sequence.

Table 1: Representative Damping Factors of Various Polymeric Laminates

Material	Fiber Orientation	Modulus (10^6 psi)	Damping Factor η
Mild Steel	-	28.0	0.0017
6061 Al alloy	-	10.0	0.0009
E-glass-epoxy	0°	5.1	0.0070
Boron-epoxy	0°	26.8	0.0067
Carbon-epoxy	0°	27.4	0.0157
	22.5°	4.7	0.0164
	90°	1.0	0.0319
	[0 / 22.5 / 45 / 90]s	10.0	0.0201

Nanomaterials continue to be applied to increasingly complex and intelligent controls systems for both machinery and structures (Ajayan et all 2006). Extensive research in nanotechnology has been conducted, but its results need to be refined, especially with regards to manufacturing and production techniques (Breuer and Sundararaj 2004). Currently, there are numerous research projects exploring diverse manufacturing techniques to produce functional and affordable nanocomposites. However, in pursuing traditional composite manufacturing strategies while incorporating nanoparticles such as carbon nanofiber, many nanocomposite manufacturing techniques

are incurring problems with even dispersion of nanofibers within the composite matrix. This significantly compromises the quality of the final product (Guo et al, 2006).

Viscoelastic materials are popular for damping applications. There are two principal approaches currently being used to achieve better damping properties. The first method involves the use of viscoelastic polymer-based tape. Carbon fiber reinforced polymer tape is commonly used to support existing structures with vibration absorption. However, the tape possesses increased weight, increased volume, propensity for de-bonding (peeling), and most importantly, poor high-temperature performance.

The second method involves nanofiller-modified epoxy films. In this method, nanofillers are dispersed within epoxy resin and applied to existing structures as a thin layer of film. One disadvantage to the approach is the limitations of nanofiller dispersion. At higher concentrations, nanofiller dispersion is uneven and results in a film with random concentration throughout. Furthermore, many nanofillers lack the high aspect ratio belonging to nanofibers. The lower aspect ratio results in decreased damping.

New strategies in nanocomposite manufacturing must be researched. Among the properties to be explored, the ability to damp vibration is of utmost importance because un-damped vibration not only affects the comfort of the user through noise and movement, but can also catastrophically compromise the safety of a structure.

The research to achieve better damping properties presented in this thesis attempts to correct the downfalls of the current approaches. Nanocomposites produced through VARTM are tested against traditional composite plates for their damping properties. Using sheets of CNF paper as well as individually dispersed nanofibers, this method is a good prospect in the pursuit of affordable nanocomposites possessing superior damping.

2.3 Isothermal Curing

2.3.1 Epoxy Resins

Epoxy resins are thermosetting polymers that, before curing, have one or more active epoxide or oxirane groups at the ends of the molecule and a few repeated units in the middle of the molecule. Chemically, they can be any compound that have one or more 1,2-epoxy groups and can convert to thermosetting materials. They exist either as liquids with lower viscosity or as solids. Through the ring opening reaction, the active epoxide group in the uncured epoxy can react with many curing agents or hardeners that contain hydroxyl, carboxyl, amine, and amino groups.

Compared to other materials, epoxy resins have several unique chemical and physical properties. Epoxy resins can be produced to have excellent chemical, heat, and electrical resistance, good adhesion, low shrinkage, and good mechanical properties, such as high strength and toughness. These desirable properties result in epoxy resins having wide markets in industry, packaging, aerospace, and construction. They have found notable applications as bonding and adhesives, protective coatings, electrical laminates, apparel finishes, fiber-reinforced plastics (FRPs), flooring, and composite pipes.

Most customary epoxy resins are prepared from bisphenol A and epichlorohydrin. For example, the most commonly used epoxy resins are diglycidyl ethers of bisphenol A. Other types of epoxy resins are glycidyl ethers of novolac resins, phenoxy epoxy resins, and aliphatic epoxy resins. Glycidyl ethers of novolac resins and phenoxy epoxy resins usually have high viscosity and better high temperature properties, while aliphatic epoxy resins have low viscosity and low glass transition temperatures.

2.3.2 Curing Agents

Curing agents play an important role in the curing process of epoxy resin because they relate to the curing kinetics, reaction rate, gel time, degree of cure, viscosity, and final properties of the cured products. Thus many researchers have been studying the effects of curing agents on the curing process.

The first type of curing agents includes active hydrogen compounds and their derivatives. Compounds with amine, amides, hydroxyl, acid or acid anhydride groups belong to this type. They usually react with epoxy resin by polyaddition to result in an amine, ether, or ester. Aliphatic and aromatic polyamines, polyamides, and their derivatives are the commonly used amine type curing agents. The aliphatic amines are very reactive and have a short lifetime. Their applications are limited because they are usually volatile, toxic, or irritating to eyes and skin and thus cause health problems. Compared to aliphatic amine, aromatic amines are less reactive, less harmful to people, and need higher cure temperature and longer cure time. Hydroxyl and anhydride curing agents are usually less reactive than amines and require a higher cure temperature and curing time. Polyphenols are the more frequently used hydroxyl type curing agents. Polybasic acids and acid anhydrides are the acid and anhydride type curing agents that are widely used in the coating field.

The second type of curing agent includes anionic and cationic initiators. They are used to catalyze the homopolymerization of epoxy resins. Molecules, which provide an anion such as tertiary amine, secondary amines, and metal alkoxides, are the effective anionic initiators for epoxy resins. Molecules that can provide a cation, such as the halides of tin, zinc, and iron are the effective cationic initiators.

The third type of curing agent is called reactive crosslinkers. They usually have higher equivalent weights and crosslink with the second hydroxyls of epoxy resins or by self-condensation. Examples of this type of curing agent are melamine, phenol, and urea formaldehyde resins.

Among the three types of curing agents, compounds with active hydrogen are the most frequently used curing agents and have gained commercial success. Most anionic and cationic initiators have not been used commercially because of their long curing cycles and other poor cured-product properties. Crosslinkers are mainly used as surface coatings and usually are cured at high temperatures to produce films having good physical and chemical properties.

2.3.3 Curing Reactions

The curing reaction of epoxide is the process by which one or more kinds of reactants, with or without the catalysts, are transformed from low molecular weight to a highly crosslinked structure. The epoxy resin contains one or more 1,2-epoxide groups. Because an oxygen atom has a high electronegativity, the chemical bonds between oxygen and carbon atoms in the 1,2-epoxide group are the polar bonds, in which the oxygen atom becomes partially negative, whereas the carbon atoms have become partially positive. Because the epoxide ring is strained (unstable), and polar groups (nucleophiles) can attack it, the epoxy group is easily broken. It can react with both nucleophilic curing reagents and electrophilic curing agents. The curing reaction is the repeated process of the ring-opening reactions of epoxides, adding molecules and producing a higher molecular weight and finally resulting in a three-dimensional structure. The chemical structures of the epoxides have an important effect on the curing

reactions. Tanaka and Bauer (1988) provide details about the relative reactivity of the various epoxides with different curing agents and the orientation of the ring opening of epoxides. It was concluded that the electron-withdrawing groups in the epoxides would increase the rate of reaction when cured with nucleophilic reagents, but would decrease the rate of reaction of epoxides when cured with electrophilic curing agents. Many curing agents may be used to react with epoxides; but for different curing agents, there exist different mechanisms of the curing reaction. Even for same epoxy resin systems, the cure mechanism may be different for the isothermal and dynamic cure processes.

Xu and Schlup (1988) studied the curing mechanism of epoxy resin/amine system by near-infrared spectroscopy. They pointed out that the etherification during the epoxy resin cure was significant only at certain reaction conditions such as at a high curing temperature and for only some epoxy resin/amine systems. The main curing reactions were also used by other researchers in the different epoxy resin/amine systems (Gonis, 1999; Laza et al., 1998). Grenier-Loustalot and Grenier (1992) studied the crosslinking mechanism and kinetics of carbon and glass fiber reinforced epoxy resin by several methods. They found that the presence of the carbon and glass fibers does not affect the reaction mechanisms.

CHAPTER 3.

RESEARCH METHODS

3.1 Manufacturing of Nanocomposites

Nanocomposites are produced quickly and economically in one of two basic fashions, Vacuum Bag Molding (VBM) or Vacuum Assisted Resin Transfer Molding (VARTM). The former involves injecting liquid resin into multiple layers of textile-like fiber preforms, while vacuum-sealed within a thin plastic bag-like apparatus. The resin-infused layers of fiber mats are kept under high pressure, and are consequently cured at room temperature. A resin that is able to cure at room temperatures must be chosen in order to use this production process. VARTM, however, employs the use of a closed mold in stead of thin plastic bagging. This allows the infused fibers to cure in an oven. This is necessary for the use of epoxy resin, which only cures at high temperatures. The VARTM method is utilized for all of the nanocomposites in this research.

The process for producing a 10 inch x 10 inch x 1/8 inch VARTM formed nanocomposite plate begins with the placement of 5 to 15 layers (depending on the fiber) of fiber preform mats into a closed aluminum mold. A total of 15 plain-woven bidirectional continuous carbon fiber mats were used for each of the composite test samples discussed in this thesis. The carbon fiber sheets were arranged in a pattern that evenly distributed their mechanical properties across the length and width directions of the plate. Each sheet was rotated 45° from the previous sheet's orientation; with the initial layer having an angle of 0° from its x-axis. This overall orientation can be depicted in shorthand by stating its laminate code. This code implies that each layer

consists of an identical material at identical thicknesses. Each ply of the fiber sheets can be represented by its orientation angle, and separated from the other plies by a slash sign. Furthermore, if an identical orientation pattern is repeated, the number of times that it repeats can be written in subscript outside of the brackets. This particular laminate can be represented by $[0 / 45 / 90]_5$. Each layer of this bidirectional laminate is rotated 45°, and is repeated 5 times for a total of 15 layers. This number of layers is necessary to fill the mold cavity, which is 1/8 inch thick.

In addition to placing the fiber layers into the mold cavity, a mold release agent was used to coat the inner surfaces of the cavity. This honey-wax-like coating is designed to keep the composite plate from sticking to the surface of the mold during the curing process. Once the fiber layers and release agent were placed onto the mold, a rubber gasket was placed around the outside of the inner cavity, and sealed into place. The mold was closed up, and bolted tight. The mold's cavity was then vacuum sealed, and injected with resin at 60 psi of pressure. Once the cavity was filled with resin, a valve was used at both the inlet and outlet to trap the high pressure within the mold. After which, the mold was placed in an oven until curing was completed.

There are still, however, a number of design variables to consider before being able to produce a high quality nanocomposite. A chart illustrating the leading design variables and their related processing issues can be seen in Figure 4. The principal design parameters to consider in this production include curing temperatures, initial mold and fiber temperatures, resin injection temperature and pressure, injection technique, and the fiber structure of the nanocomposite. These variables may affect the curing reaction of the resin, viscosity of the resin, preform permeability, or mold filling characteristics.

Potential issues that may occur in the produced nanocomposite from the improper design of these parameters may include, a low degree of cure, non-uniform cure, incomplete mold filling, dry spot formation, or void formation.

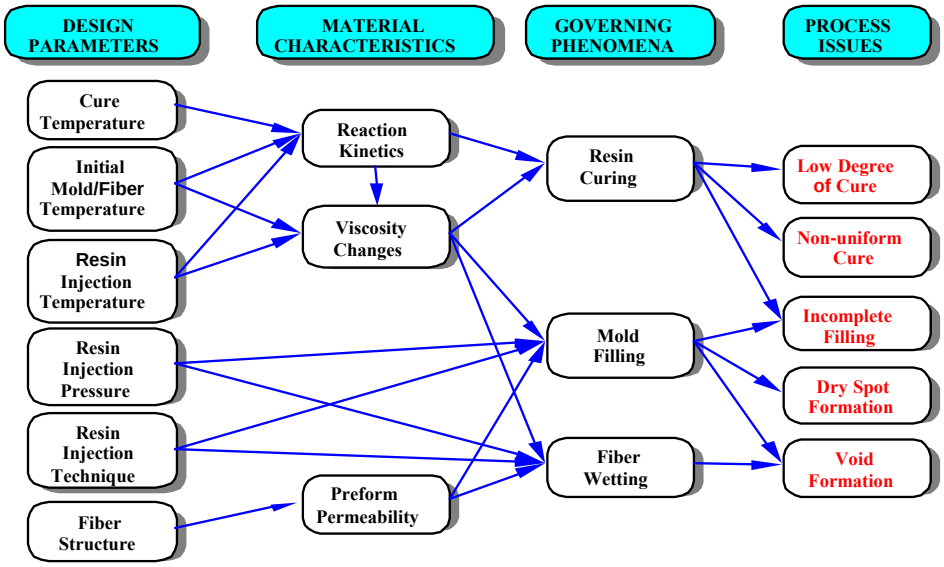

Figure 4: Design variables vs. process issues

3.1.1 Dispersion Techniques of Carbon Nanofibers

The particular CNFs used for this research were PR-25-OXT (oxidized) carbon nanofibers. The as-received carbon nanofiber powder needed to be dispersed before adding it to the resin. The desired amount of carbon nanofibers is determined by weight percent of the resin. That amount of CNF is added to a solvent within a 1000 ml glass beaker. Acetone was used as the solvent. This allowed for any excess solvent trapped within the CNF to easily evaporate. The amount of solvent used is dependant on the amount of CNF. 400 ml of solvent was used for every 1 gram of CNF. A dispersion agent was also added to the solvent. 1 single drop of Triton dispersion agent was used for every 100 ml of solvent.

This mixture was then sonicated using a high intensity sonicator (600-watt Sonicator 3000 from Misonix Inc.) for a prescribed amount of time. Once again, the sonication time was dependent on the amount of solvent. 20 minutes of sonication was necessary for every 1 gram of CNF. The sonicated solution is then filtered with a 0.4 μm hydrophilic polycarbonate membrane with the aid of a vacuum pump. Once filtered, a disc-like collection of carbon nanofibers is produced. These CNFs are then dispersed within the resin by means of a high speed mechanical mixer. Mixing 10 minutes for every 300 grams of resin sufficiently disperses the carbon nanofibers.

3.1.2 Manufacturing of Carbon Nanofiber Paper

The process of manufacturing the CNF in the form of paper is similar to preparing them for dispersion within resin. The process begins with as-received carbon nanofiber (CNF) powder. The as-received CNF powder was ground in a mortar with a small amount of ionized water. After grinding, they were transferred into a 500 ml glass beaker. 400 ml of solvent was then added to the powder. The mixture was subsequently sonicated using a high intensity sonicator (600-watt Sonicator 3000 from Misonix Inc.) for 20 minutes with 30-50 watts of power. After the solution and probe were cooled to room temperature, the solution was sonicated for another period of 20 minutes under identical conditions. The as-prepared solution was allowed to settle overnight. 300 ml of upper suspension was collected and treated with the ultrasonic sonicator for 10 minutes before being filtered with 0.4 μm hydrophilic polycarbonate membrane with the aid of a vacuum pump and high-pressure air. The as-prepared carbon nanopapers (CNPs) were dried in a 120°C oven for 2 hours. After which, a single sheet of carbon nanopaper is ready for use.

3.1.3 Resin Injection Techniques

Proper resin flow through dry fibers is critical in producing void-free parts and good fiber wet-out. In thermoset resins, curing may take place simultaneously with resin flow, and if the resin viscosity rises too rapidly due to curing, its flow may be inhibited, causing voids and poor interlaminar adhesion.

The Vacuum Assisted Resin Transfer Molding (VARTM) process is used in conjunction with a 12 inch x 12 inch x 2 inch aluminum mold. Once each layer of the carbon fiber mats and release agent were placed onto the mold, a rubber gasket was positioned around the outside of the inner 10 inch x 10 inch x 1/8 inch cavity, and sealed into place. The mold was closed up, and bolted tight at each of its four corners.

The inlet of the mold was connected to a pressure vessel which contained the resin sample. That pressure vessel was also connected to a high pressure line. On the other side of the mold, the outlet was connected to a vacuum pump. This set-up can be seen in Figure 5.

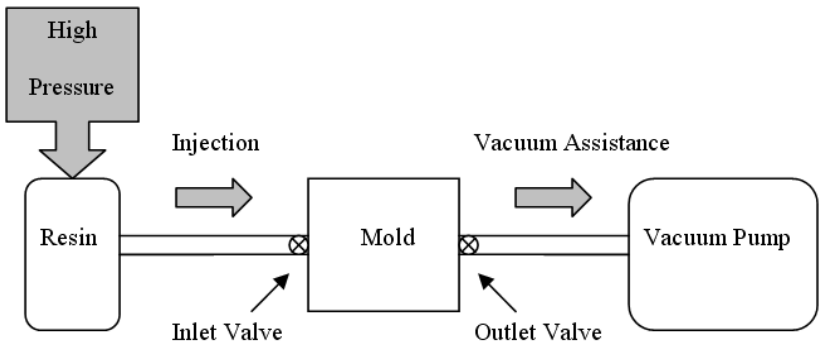

Figure 5: Schematic of mold injection apparatus

The mold's cavity was then vacuum sealed. This will aid the resin in permeating as much of the fiber mats as possible. This will reduce the number of voids in the end product, and is commonly referred to as fiber wet-out. Once a vacuum is formed within

the cavity, it is injected with resin under high pressure at 60 psi. The high pressure pulls the resin into the mold cavity. Once the cavity was filled with resin, a valve was used at both the inlet and outlet to trap the high pressure within the mold. After which, the mold was cut from its inlet and outlet lines, and placed in an oven at 170° for 2 hours, at which curing was completed.

3.2 Isothermal Curing of Resin

Several techniques have been used to study the curing process of epoxy resins. They can be classified as either chemical or physical methods. Fourier transform infrared spectroscopy (FTIR), nuclear magnetic resonance (NMR), infrared spectroscopy and radiochemical methods are traditionally considered as chemical-based approaches. Differential scanning calorimetry (DSC), thermal scanning rheometry (TSR), and thermomechanical analyzer (TMA) are considered as physical methods. These chemical and physical methods are sometimes used together to analyze the curing mechanism. In the following experiments, two physical methods were employed to analyze curing behavior. A rheological (viscosity-based) and differential scanning calorimetry (thermal-based) analyses were conducted in order to characterize the curing process.

3.2.1 Rheological Analysis

Epoxy resins exhibit both viscous and elastic properties. During the curing process, their viscosity increases rapidly in the gel region. The viscosity of a resin can be related to its degree of cure. Rheological equipment can be used to measure the viscosity of epoxy resins while curing. Hinrichs (1983) discussed the requirements for a rheological instrument to successfully measure the rheological properties of the polymer.

The viscosity of the polymer materials can be measured in the continuous rotation or oscillation mode.

A series of rheological experiments were conducted in order to illustrate a trend in curing or gel times with respect to factors such as curing temperature and resin CNF content. In these experiments, a rotating spindle was suspended in a 300 ml sample of epoxy resin. The resin is kept at an isothermal temperature, as a viscometer continuously measures its viscosity throughout the curing process. Pure epoxy resin was tested along with 0.25, 0.5, 0.75, and 1.0 weight percent of CNF. The viscosities of these epoxies were recorded while curing at temperatures of 75°, 100°, and 125°C. These viscosity measurements were examined to characterize each epoxy's curing behavior.

3.2.2 DSC Analysis

Differential scanning calorimetry is a quantitative differential thermal analysis technique (Hatakeyama and Quinn, 1994). During measurement with DSC, the temperature difference between a sample and a reference is measured as a function of either temperature or time. This difference is considered to be proportional to the change in heat flux.

In the study of curing kinetics of epoxy resins, it is assumed that the degree of cure can be related to the heat of the reaction. Both isothermal and dynamic methods can be employed to determine the kinetic parameters with DSC. For the isothermal method, the sample is quickly heated to the preset temperature. The system is held at that temperature and the instrument records the change of heat flux as a function of time. For the dynamic method, the heat flux is recorded when the sample is scanned at a constant

heating rate from low temperature to high temperature. The area under the heat flux curve and above the baseline is calculated as the heat of reaction.

A series of experiments were conducted in order to illustrate the degree of cure of epoxy resin with respect to curing temperature and resin CNF content. A 10 mg sample of epoxy resin was isothermally cured within a small capsule, while an empty reference capsule was simultaneously heated at the same temperature. The measured difference in heat flux, or heat generation, between the two capsules was used to determine the rate of cure for each of the resin samples.

The amount of heat released, H, during the constant curing of epoxy resin is equal to the area under the rate of heat flux vs. time curve. This quantity is expressed as,

$$H = \int_0^t \left(\frac{dQ}{dt}\right)_i dt \qquad \textbf{(1)}$$

where $\left(\frac{dQ}{dt}\right)_i$ is the rate of heat generation in an isothermal experiment at any time t. The degree of cure, α_c, of the epoxy resin at any time can be calculated by the following,

$$\alpha_c = \frac{H}{H_R} \qquad \textbf{(2)}$$

where H is the heat generation at that specific time, and H_R is the total heat generation to complete the curing reaction. This ratio plotted against time describes the current point at which the resin sample is in its overall curing process.

3.3 Flow Visualization

3.3.1 RTM Process Modeling and Simulation

3.3.1.1 Governing Equations

The resin flow through fiber mats has been modeled using Darcy's law, which was derived from Newtonian fluids through a porous medium. This equation relates the volumetric resin-flow rate q per unit area to the pressure gradient that causes the flow to occur. For one-dimensional flow in the x direction, Darcy's equation is described as,

$$q = -\frac{P_0}{\eta}\left(\frac{dp}{dx}\right) \tag{3}$$

Where P_0 is the permeability, η is the viscosity, and $\left(\frac{dp}{dx}\right)$ is the pressure gradient, which is negative in the direction of flow. The permeability is described by the following equation known as the Kozeny-Carman equation,

$$P_0 = \frac{{d_f}^2}{16K}\,\frac{(1 - v_f)^3}{{v_f}^2} \tag{4}$$

where d_f is the fiber diameter, v_f is the fiber volume fraction, and K is the Kozeny constant. In order for process optimization and control of the processing conditions, a process model has been developed based on the fundamental mechanics. Darcy's equation can describe resin flow in the fiber preform with acceptable accuracy in tensor notation in three dimensions:

$$\vec{V} = -\frac{[K]}{\eta} \cdot \nabla P \tag{5}$$

where $\vec{V}$ is the velocity of the resin flow, η is the viscosity of the resin, $[K]$ is the permeability tensor of the fiber preform, and P is the pressure.

As the resin is incompressible, the continuity equation is given by:

$$\frac{\partial u}{\partial x} + \frac{\partial v}{\partial y} + \frac{\partial w}{\partial z} = 0 \tag{6}$$

Equation 5 and *6* are combined and integrated over a control volume to yield the following expression:

$$\iint_s \frac{1}{\eta} \begin{bmatrix} n_x & n_y & n_z \end{bmatrix} \begin{bmatrix} k_{xx} & k_{xy} & k_{xz} \\ k_{yx} & k_{yy} & k_{yz} \\ k_{zx} & k_{zy} & k_{zz} \end{bmatrix} \begin{bmatrix} \frac{\partial P}{\partial x} \\ \frac{\partial P}{\partial y} \\ \frac{\partial P}{\partial z} \end{bmatrix} ds = 0 \tag{7}$$

where n_x, n_y, and n_z are the components of the vector normal to the surface of the integrated volume, k_{ij} are the components of the permeability tensor $[K]$ defined in a three-dimensional Cartesian coordinate system.

The initial and boundary conditions are as follows.

At the injection gate:

$$u_{gate} = u_0 \tag{8}$$

At the mold wall:

$$\frac{\partial P}{\partial n_{wall}} = 0 \tag{9}$$

At the flow front region:

$$P_{front} = 0 \tag{10}$$

Solutions to *Equation 7* along with the boundary conditions [Equations 8 – 10] yield the resin flow front location as well as pressure distribution as a function of time.

3.3.1.2 Numerical Method

Equation 7, which is based on the mass balance, is the control equation for solving the problems of flow through anisotropic porous media. The pressure is the final parameter in the control equation. *Equation 7* is used to solve the transient flow field during mold filling, although the equation is steady, and the mold filling is not. The mold filling can be regarded as a quasi-steady-state process by assuming a steady state condition at each time. In other words, the problem is solved by considering the transient solution to be a sequence of steady state solutions separated by many small time increases. The assumption is reasonable because the inertia is negligible. The Control Volume Finite Element Method (CVFEM) can be used to solve *Equation 7* numerically.

The RTM mold filling process is a moving boundary problem, in which the computational domain changes continuously at each time step. The control volume finite element method is used to solve this problem without mesh regeneration. In the CVFEM, the entire computational domain is discretized into a number of elements. By connecting the centroids of the elements and the midpoints of the element borders, the computational domain can be divided again into a number of polygonal control volumes.

Since the thickness of the RTM part is often much smaller than the length or width, the resin flow in the mold is considered to be a two-dimensional problem. *Equation 7* can be rewritten as:

$$\int_c h_z \begin{bmatrix} n_x & n_y \end{bmatrix} \begin{bmatrix} k_{xx} & k_{xy} \\ k_{yx} & k_{yy} \end{bmatrix} \begin{bmatrix} \frac{\partial P}{\partial x} \\ \frac{\partial P}{\partial y} \end{bmatrix} dL = 0 \quad \textbf{(11)}$$

where h_z is the thickness of the RTM part.

Using linear shape function for a 3-node triangular element, an approximation of *Equation 11* can be given as:

$$P = a_0 + a_1 x + a_2 y \quad \textbf{(12)}$$

where x and y are local coordinates. The local coordinate system is shown in Figure 6. The values of a_0, a_1, and a_2 depend on the corresponding coordinates and node pressure.

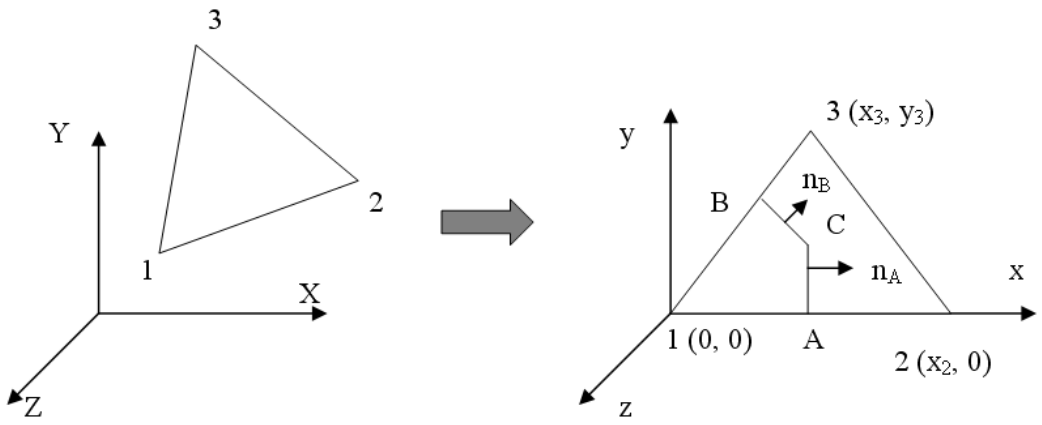

Global coordinate system Local coordinate system

Figure 6: Transformation of 2-D coordinate system for a triangular element

The pressure gradient in the element can be computed as follows:

$$\begin{bmatrix} \frac{\partial P}{\partial x} \\ \frac{\partial P}{\partial y} \end{bmatrix} = \begin{bmatrix} -\frac{1}{x_2} & \frac{1}{x_2} & 0 \\ -\frac{1}{y_3}+\frac{x_3}{x_2 y_3} & -\frac{x_3}{x_2 y_3} & \frac{1}{y_3} \end{bmatrix} \begin{bmatrix} P_1 \\ P_2 \\ P_3 \end{bmatrix} \tag{13}$$

Substituting *Equation 13* into *Equation 11* and integrating we obtain the equation within a small control volume, which is composed of 3-node triangular elements.

$$\sum_{t=0}^{m} \left(\sum_{X=A,B} \begin{bmatrix} w_{X1} & w_{X2} & w_{X3} \end{bmatrix} \begin{Bmatrix} P_1 \\ P_2 \\ P_3 \end{Bmatrix} \right)_t = 0 \tag{14}$$

where m is the total number of elements in a control volume, w_{X1}, w_{X2}, and w_{X3} are coefficients for the pressure of node.

For a 4-node quadrilateral element, the pressure distribution of the quadratic element is represented by

$$P = N_i P_i \tag{15}$$

where $N_i = \frac{1}{4}(1+\zeta_i\zeta)(1+\eta_i\eta)$, $\zeta_i = -1,+1,+1,-1$, and $\eta_i = -1,-1,+1,+1$.

Similarly, we get the equation within a small control volume composed of 4-node quadrilateral elements.

$$\sum_{t=0}^{m} \left(\sum_{X=A,B} \begin{bmatrix} w_{X1} & w_{X2} & w_{X3} & w_{X4} \end{bmatrix} \begin{Bmatrix} P_1 \\ P_2 \\ P_3 \\ P_4 \end{Bmatrix} \right)_t = 0 \tag{16}$$

Then a set of linear algebraic equations can be obtained by writing *Equation 16* for all control volumes in the computational domain. Solving the linear algebraic equations

together with the appropriate boundary conditions, we can obtain the pressure of each node in the flow field.

After the pressure field is determined, the velocity field can be calculated according to Darcy's law. If a control volume is completely filled $(f = 1)$, it is classified as the main flow region. If a control volume is empty $(f = 0)$, it belongs to the empty region. The control volumes partially filled with the resin is presented as the flow front region $(0 < f < 1)$. For a selected time increment, the volume of resin into control volumes at the flow front region is calculated and added to the original resin volume in the control volume at the flow front region. If the total resin volume in a control volume is equal to the volume of the control volume, that control volume is considered "full." The mold filling is regarded as a quasi-steady-state process by assuming a steady state condition at each time step. Thus, the time increment is determined in such a way that minimum control volumes will be filled in each time step to ensure the stability of the quasi-steady-state approximation. After the flow front region at each time step is updated, another pressure computation is performed for the main flow region. The procedure is repeated until the whole mold cavity is filled.

3.3.2 Experimental Injection

In order to corroborate the results from the numerical simulation, physical RTM injections were performed. A custom-designed mold was manufactured for the purpose of capturing real-time flow visualization. The base of the mold was constructed out of aluminum, while the lid was built from transparent polycarbonate, in order to see the contents of the mold cavity. The cavity measured 10 inches x 8 inches x 1/8 inch, with a 1/8 inch diameter inlet at the edge of the aluminum base, located at the center of one of

its 10 inch sides. A single outlet was similarly placed on the other side of the mold, adjacent to the inlet.

Epoxy resin containing 0, 0.25, 0.5, 0.75, and 1.0 weight percent CNF were each injected at 60 psi into the fiber-filled mold at room temperature and video recorded to visually analyze their flow characteristics. These mold-filling experiments were conducted at room temperature since the transparent polycarbonate lid cannot tolerate the high curing temperatures of epoxy resin. Also, 4 layers of bidirectional glass fiber mats were used in stead of 15 layers of bidirectional carbon fiber. The flow pattern through carbon fiber mats would be indistinguishable since both the CNF-modified epoxy resin and the carbon fiber sheets are black. Time-lapse images were created from each of the video recordings and compared against the ideal computer simulations.

Two types of mold injections were considered in the simulation and visualization process. The first type of injection used is called point injection. In this type, resin is injected into the mold cavity at a single inlet. The resin therefore fills the cavity in a radial fashion. The second type is termed line injection. In this type of injection, a single inlet is again used. However, it differs in that the fiber sheets do not entirely fill the mold cavity. A ¼ inch gap is left on the side of the mold cavity containing the inlet, allowing the injected resin to fill this gap before permeating the fiber sheets. Thus, the flow pattern fundamentally changes from a radial expansion to a linear flow from the inlet side of the mold cavity to its adjacent side. This technique is useful for injecting resins with higher CNF content and therefore higher viscosities.

3.4 Damping Testing

A series of nanocomposites fabricated with the VARTM process were tested for their damping abilities by three means of experimentation. Dynamic mechanical analysis, piezoelectric vibration testing, and piezoelectric acoustic testing each provided data with which to determine the damping abilities of the fabricated nanocomposites. Nanocomposites manufactured with the CNF-modified epoxy were tested using dynamic mechanical analysis and piezoelectric vibration analysis. Traditional CFRP composites affixed with a single sheet of CNF paper were tested using piezoceramic patches. These patches were used to examine both vibration and acoustic damping effects.

3.4.1 Dynamic Mechanical Analysis

Damping properties of nanocomposite plates, manufactured by Vacuum Assisted Resin Transform Molding, were determined by means of dynamic mechanical analysis (DMA). Four VARTM formed nanocomposite plates were manufactured with epoxy resin containing different weight percentages of carbon nanofibers. This CNF-modified epoxy resin was injected between 15 layers of bidirectional woven carbon fiber sheets. The four carbon fiber reinforced polymer (CFRP) plates were constructed from 0, 0.25, 0.5, and 1.0 weight percent CNF-modified epoxy resin. 20 mm x 6 mm x 4 mm samples were cut from each of the plates and tested using the DMA apparatus shown in Figure 7. The testing apparatus consisted of the dynamic mechanical analyzer, with the cylindrical test chamber located at its core, and the data acquisition system connected to a PC in order to record the experimental data.

Figure 7: DMA testing apparatus

Each sample is placed in the test chamber in a manner described in Figure 8. Each end of the test sample is held stationary, while the temperature of the chamber increases from 25 to 250 °C at a rate of 5 °C/min. Thermal expansion causes an internal strain in the test sample. This strain is measured at its center as deflection in the thickness of the test sample.

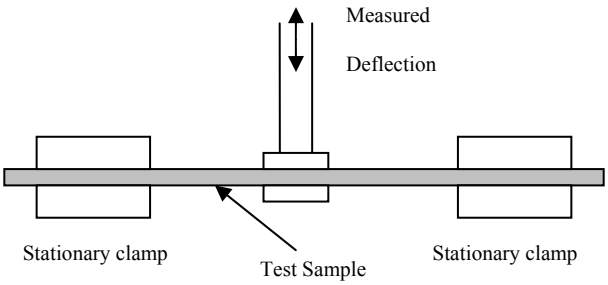

Figure 8: DMA test sample positioning inside the testing chamber

Both the elastic modulus (storage modulus) and the viscous modulus (loss modulus) are obtained from the strain values recorded during the testing process. Theses modulus values can then be used to obtain the damping ratio of the test sample.

3.4.2 Vibration Damping

The damping properties of four additional nanocomposite plates were determined by analyzing the vibration response to sweep sine excitations using piezoceramic patches. The patches were used as both an actuator and a sensor. Four 10 inch x 10 inch x ¼ inch VARTM-formed nanocomposite plates were fabricated with varying weight percentages of carbon nanofibers dispersed between layers of fiberglass mats. The weight percentage of carbon nanofiber and mass of the nanocomposite plates are summarized in Table 2.

Table 2: Properties of Nanocomposite Plates

Sample	Weight % CNF	Mass (g)
DS-1	0.0%	764
DS-2	0.5%	753
DS-3	1.0%	749
DS-4	1.5%	742

The difference between the fiberglass laminates containing CNF-modified epoxy resin is visually apparent. The epoxy resin without CNF modification appears translucent. The VARTM-formed glass fiber composite plate without CNF-modified resin is seen in Figure 9a, whereas a plate containing CNF-modified resin can be seen in Figure 9b.

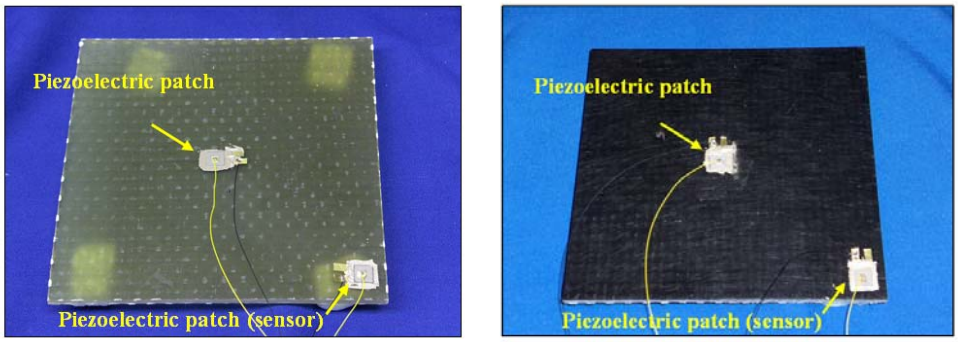

a) b)

Figure 9: Plate a) with and b) without CNF-modified epoxy resin

To set up this experiment, 10 mm x 10 mm lead zirconate titanate (PZT) piezoceramic patches were cut from a larger PZT sheet. A schematic drawing of a completed, bonded PZT actuator/sensor is presented in Figure 10. CircuitWorks CW2400 Conductive Silver Epoxy was mixed as the bonding element between the PZT patches and the nanocomposite plate. Using the conductive epoxy, one PZT patch was surface bonded to the center of the plate. This patch was to act as the actuator. Two thin, 3 mm x 5 mm strips of brass sheeting were also bonded to the nanocomposite plate by the epoxy used to bond the PZT patch. These brass strips were used as electrodes to solder the wire leads for the data acquisition system. Using the same bonding method, a second PZT patch and pair of brass strips were bonded to the corner of the nanocomposite plate such that the PZT patch was centered at 1 inch from each neighboring edge. This patch was to act as the sensor. Next, 30 gauge wire was utilized to form electrodes to each side of the PZT patch. The thin wire minimized the effects of stiffness, and thus damping properties, of the composite plate. Using 8 inch lengths of each black and yellow insulated wire; yellow wire was soldered onto one brass electrode and black wire was soldered onto the top surface of each PZT patch. The second brass electrode is left as a back-up to any mistakes or breakages.

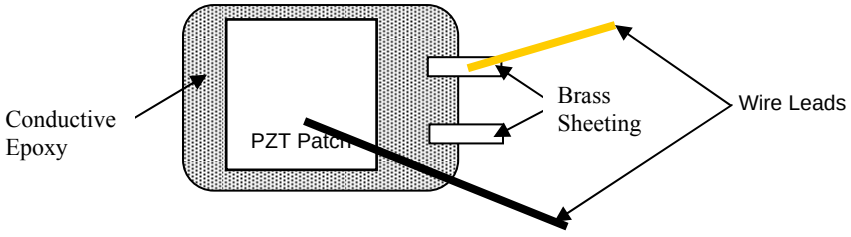

Figure 10: Completed PZT Sensor/Actuator

A dSpace data acquisition board was used to actuate and record the frequency response of the composite plate. A schematic diagram of the experimental set-up is

presented in Figure 11. The electrodes for a sensor patch in the corner of the nanocomposite plate were connected by alligator-BNC cable to the Analog to Digital Converter (ADC) channel #1 of the dSpace hub. The dSpace hub was connected to PC serial bus cable and is controlled by dSpace Control Desk and Simulink software installed on the PC. The Digital to Analog Converter (DAC) channel #1 port of the dSpace hub was then connected to the input of a Quickpack power amplifier with gain set to 20. The output of the power amplifier was then connected to the central, actuating PZT patch bonded to the nanocomposite plate. A Simulink real-time model was built to send a sweep sine excitation signal to the PZT actuator and record the frequency response of the PZT sensor. The sweep sine excitation had an initial frequency of 100 Hz and a terminating frequency of 10 kHz over a duration of 10 seconds. Since the PZT actuator has a minimum actuation voltage of 100 V, the excitation signal was scaled accordingly by the dSpace control system. As mentioned, the power amplifier had a gain of 20, while the dSpace board itself had a built-in gain of 10. Thus, the output signal from the PC to the dSpace board was approximately 0.2-V.

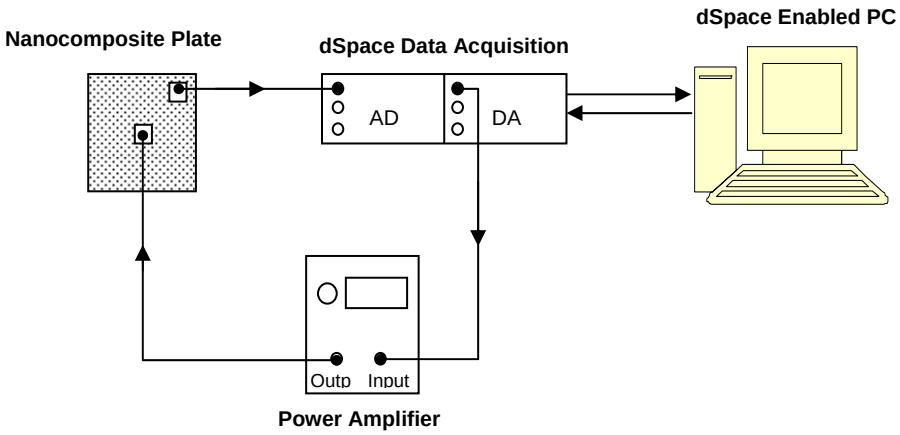

Figure 11: Schematic Diagram of Experimental Set-Up

The frequency response was captured by exciting the actuator with the sweep sine signal and recording the voltage induced in the PZT sensor by the displacement of the nanocomposite plate. Both the time and frequency of the signal were recorded with the voltage response of the PZT sensor. Using MatLab to plot the frequency response, the peak voltage responses were identified graphically through Bode plots. The frequency domain Bode plots are analyzed to determine the damping ratios of the nanocomposite plates. The half band power algorithm states,

$$2\zeta = \frac{\omega_2 - \omega_1}{\omega_n}, \tag{17}$$

where ξ is the damping ratio, ω_n is the natural frequency, and ω_1 and ω_2 are the frequencies at which there is a three decibel drop before and after the natural frequency, respectively. By identifying the peaks in the Bode plot, the natural frequency, ω_n, and the corresponding ω_1 and ω_2 were found through inspection of the frequency response.

3.4.3 Acoustic Damping

The same four 10 inch x 10 inch x ¼ inch VARTM formed glass fiber nanocomposite plates were then tested for their acoustic damping properties. Once again, their varying CNF content with respect to resin consisted of 0, 0.5, 1.0, and 1.5 weight percent. The nanocomposite plates were once again actuated with a PZT patch at its center. However, a sound level meter was used to record the acoustic response of the plate in stead of a second PZT patch.

CHAPTER 4.

RESULTS

4.1 Isothermal Curing of Resins

The isothermal curing behavior of epoxy resin containing various weight percents of CNF were documented using both rheological analysis techniques as well as differential scanning calorimetry (DSC). The resin's viscosity was recorded throughout its isothermal curing reaction with the aid of a viscometer. Similar resin samples were examined with differential scanning calorimetry to obtain their degree of cure with respect to time.

4.1.1 Rheological Analysis

The viscosities were recorded with respect to time for epoxy resin with varying amounts of CNF modification for isothermal curing temperatures of 75°, 100°, and 125°C. An exponential trendline was used to curve-fit each set of data. It can be seen from Figure 12a that the epoxy resin sample without any CNF modification, isothermally cured at 75°C, reached its gelling region after 240 minutes. The resin sample that remained heated at 100°C began to cure after 120 minutes. Lastly, the sample heated at 125°C began curing within only 30 minutes.

The viscosity readings for each of the other resin samples reflect similar results. As the curing temperature increases, the curing time or gel time decreases. Figure 12b shows the isothermal curing of 0.25 weight percent CNF-modified epoxy. The curing of the sample at 75°C is significantly delayed by the addition of CNF. It takes longer than 300 minutes for the resin to begin to gel. However, the effect of gel times at 100°C and

125°C are negligible. Figure 12c demonstrates a similar viscosity pattern. Curing at the lowest of the temperatures delays the curing, whereas the highest temperature rapidly increases the curing reaction of the resin. This continues to be demonstrated in Figure 12d and Figure 12e.

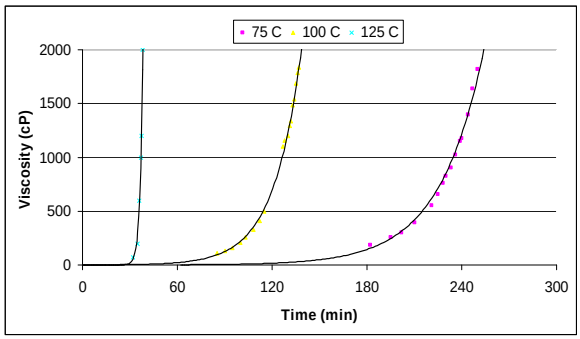

a) 0 weight percent CNF

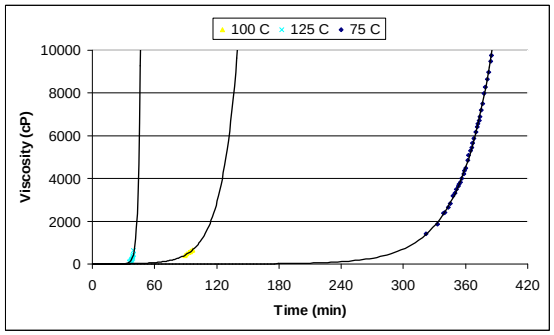

b) 0.25 weight percent CNF

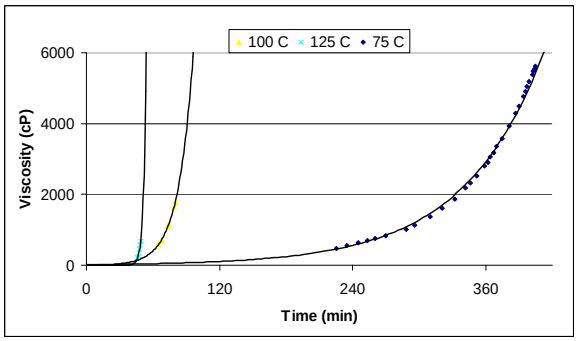

c) 0.5 weight percent CNF

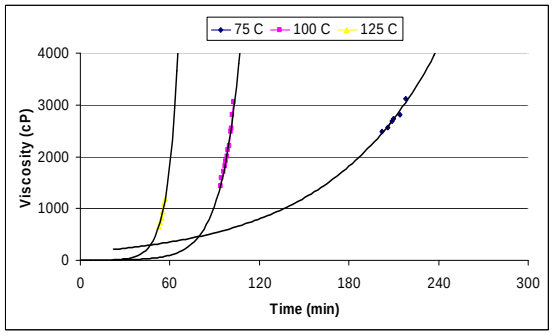

d) 0.75 weight percent CNF

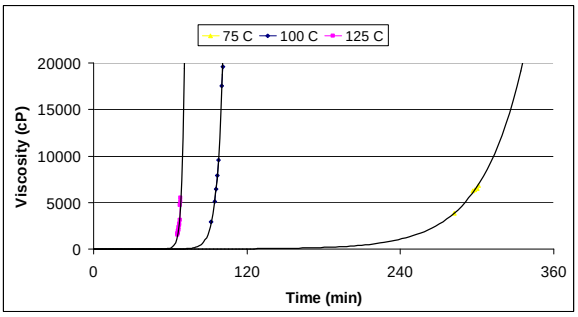

e) 1.0 weight percent CNF

Figure 12: Viscosity during isothermal curing for various weight percents of CNF

Figure 13 shows the isothermal curing of various weight percent CNF-modified epoxy resin for temperatures of 75°, 100°, and 125°C. It can clearly be seen in Figure 13c that as the weight percent of CNF-modified epoxy increases from 0 to 1.0 %, the curing time decreases.

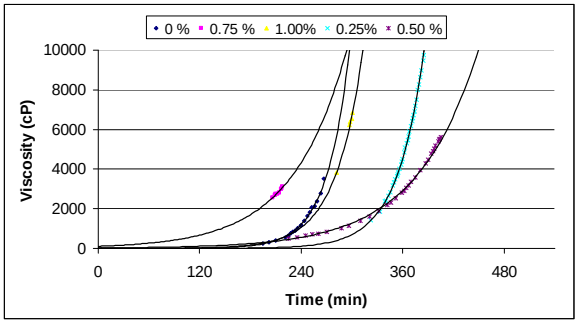

a) 75°C

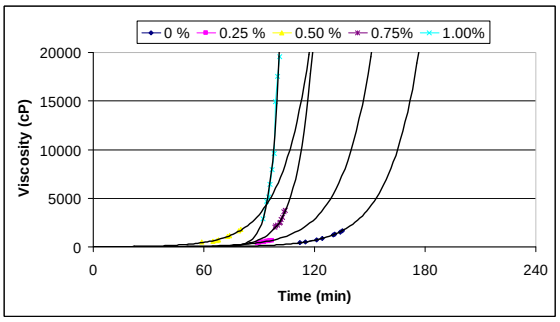

b) 100°C

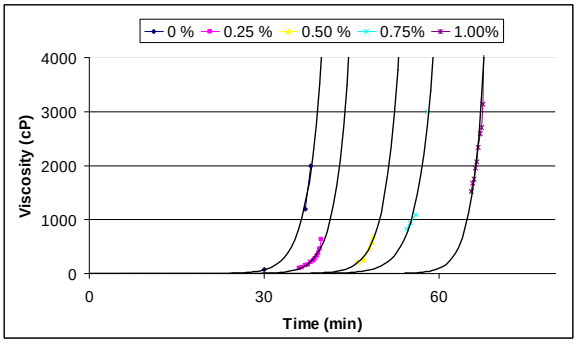

c) 125°C

Figure 13: Viscosity during isothermal curing at various temperatures

From the series of recorded viscosity measurements, initial and minimum readings were averaged for each epoxy resin according to weight percent of CNF. Table 3 contains these averaged initial and minimum viscosity values. It can be seen from the previous figures as well as the table that each of the resin samples at room temperature possesses a distinct viscosity value. This value is measured in centipoise (cP), and represents its inhibition to flow. As a reference, water has a viscosity of 1 cP. It can be

determined from the values in Table 3 that as weight percent of CNF increases in the resin, the viscosity also increases. The only sample that does not follow this trend is the 0.5 weight percent sample. This may have been due to improper CNF dispersion or disturbances in the isothermal curing process.

After initial heating, the viscosities fall drastically for every sample. The pure resin actually drops off the viscometer's scale, which read effectively as 0 cP. As the CNF content increased in the resin, the minimum viscosity also increased. The viscosity of the 1.0 weight percent resin never drops below 630 cP. This introduces a major inhibition in resin flow, even when injecting this resin at high temperatures. In the next phase of curing, the viscosity gradually increases slightly for varying times and temperatures. In the final phase of curing for most samples, the viscosities rapidly increase in an exponential manner. The resin cures so rapidly that maximum viscosity values are not recorded. This trend can be viewed in Figure 12 and Figure 13.

Table 3: Initial and minimum viscosities for various weight percents of CNF

Weight % CNF	Initial Viscosity (cP)	Minimum Viscosity (cP)
0.00%	1,175	0
0.25%	2,250	50
0.50%	19,667	148
0.75%	15,333	464
1.00 %	26,667	630

4.1.2 DSC Analysis

The series of measurements taken with differential scanning calorimetry provided data for the heat generated by the resin samples throughout the curing process. Figure 14 shows the heat generation for an isothermal curing of 0.5 weight percent CNF-modified

epoxy. The curves represent heat flow from each of the three curing resin samples at temperatures of 167°C, 177°C, and 187°C. These curves for the 0.5 weight percent samples are compared to a pure resin (0 %) sample cured at 177°C, which acts as a reference. It can be seen that the pure resin sample provides the highest amount of heat flow resulting from the curing process. Also, it can be seen that the heat flow from the 0.5 weight percent CNF-modified resin sample cured at a constant 187°C generates the least amount of heat. As the isothermal curing temperature decreases to 177°C, and then to 167°C, the heat flow emanating from the curing 0.5 weight percent CNF-modified resin increases.

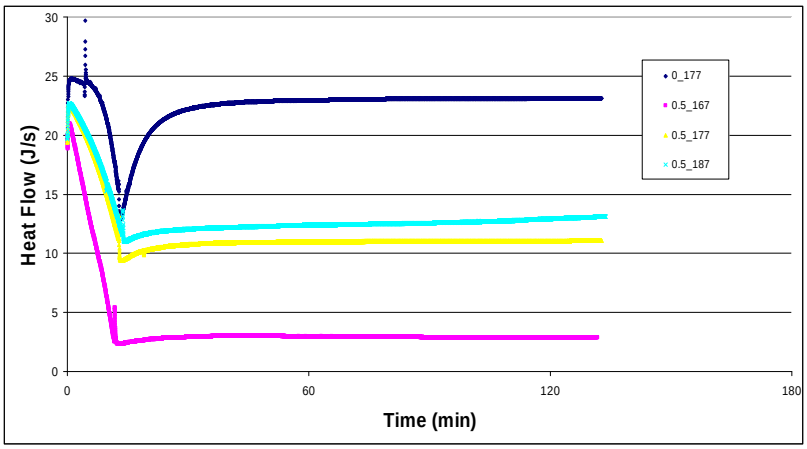

Figure 14: Heat flow for isothermal curing of 0.5 weight percent CNF

From the amount of heat released, H, during the constant curing of the epoxy resin and the total heat generation, H_R, from the entire curing reaction, the degree of cure, α_c, of the epoxy resin at any time was calculated. Figure 15 shows the degree of cure for the 0.5 weight percent CNF-modified resin samples plotted against time in a logarithmic scale. It shows the curing process primarily being activated within the first 10 minutes for each of the samples. After which, the reaction slows down. It is apparent that the CNF resin cured at 167°C achieves a higher degree of cure more quickly than the

other CNF resin samples. The CNF resin cured at 177°C doesn't reach as high of a degree of cure as it did at 167°C. The sample cured at 187°C reaches degrees of cure lower still.

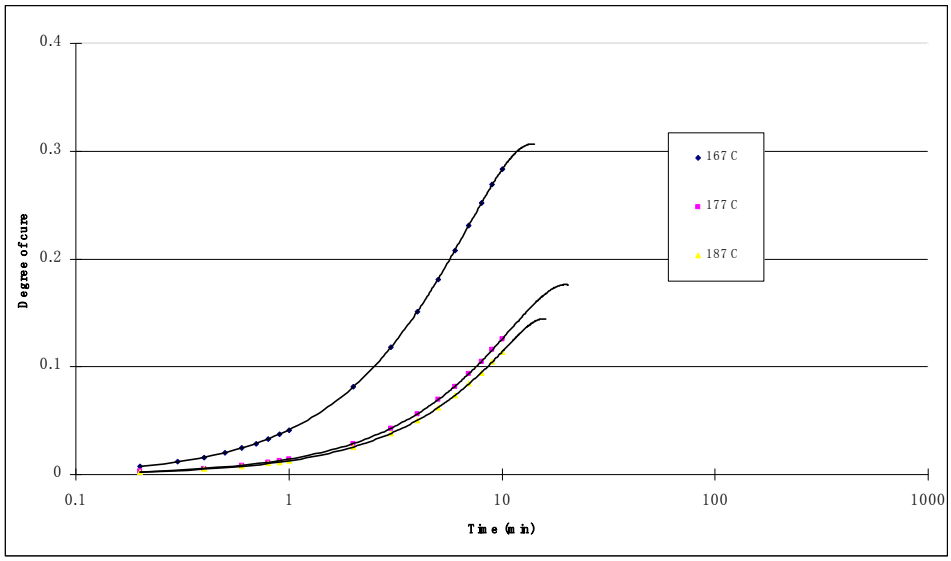

Figure 15: Degree of cure plot for 0.5 weight percent CNF

4.2 Flow Visualization Analysis

The resin flow of various CNF-modified epoxy resins through multiple-layered woven fiber mats were simulated both computationally and practically. The injection parameters of the composite mold, the multiple layers of glass fiber sheets inside the mold cavity, and the various CNF epoxy resins were used to produce a computer simulation of the flow pattern and pressure pattern within the cavity of the composite mold. The actual CNF resins were then injected into the custom-designed composite mold, and video recorded to compare against the simulated flow patterns.

4.2.1 Simulation

Figure 16 shows the simulated flow pattern and pressure pattern for a point injection. The flow begins at the inlet, which is located at the center of the bottom side of the mold. The flow then expands in a radial manner, filling the mold cavity. In the flow pattern, the cavity-filling time is represented by a color spectrum. The areas of the mold cavity marked by cooler colors represent shorter filling times, whereas the warmer colors signify longer filling times. In the pressure pattern, the pressure within the mold cavity is represented by another color spectrum. For this illustration, the higher pressures are intuitively represented by red and other warmer colors. As the color spectrum tends toward blue and the cooler colors, the pressure within the mold cavity is decreased.

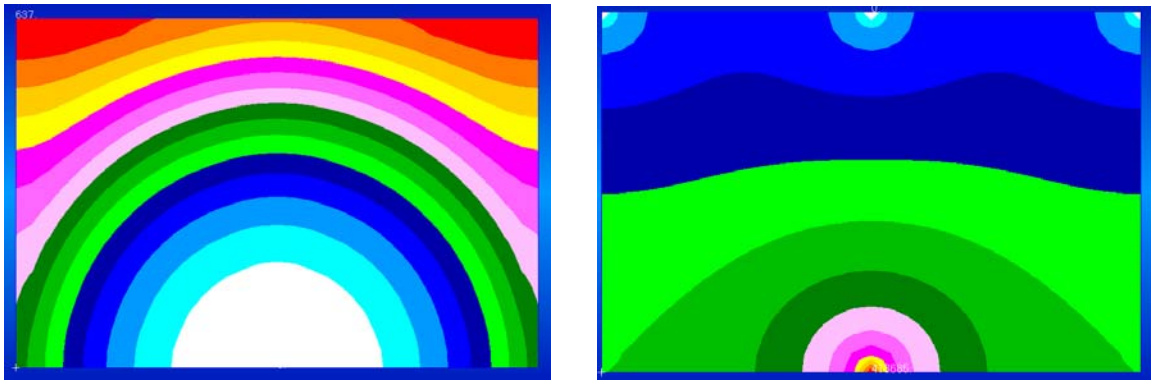

a) Flow pattern b) Pressure pattern

Figure 16: Simulated a) flow pattern and b) pressure pattern for a point injection

Figure 17 shows the simulated flow pattern and pressure pattern for a line injection. The flow once again begins at the inlet, at the center of the bottom side of the mold. However, in this case, the flow immediately fills the ¼ inch gap in the mold cavity before continuing to fill the rest of the mold. The flow and pressure patterns are therefore changed to a unidirectional flow across the mold cavity. In the flow pattern, the cavity-filling time is again intuitively represented by the same color spectrum. In the pressure

pattern, the pressure within the mold cavity is represented by another intuitive color spectrum. The pressure decreases as the as the color spectrum tends from red to white.

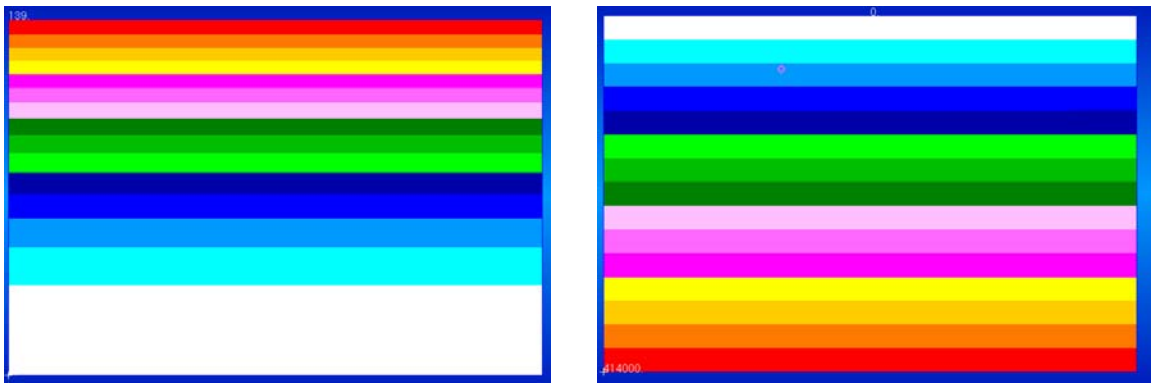

a) Flow pattern b) Pressure pattern

Figure 17: Simulated a) flow pattern and b) pressure pattern for a line injection

4.2.2 Experimental Injection

The actual epoxy resin containing 0, 0.25, 0.5, 0.75, and 1.0 weight percent CNF were each injected into the fiber-filled mold at room temperature and video recorded to compare against the simulated flow patterns. The flow pattern through the white glass fiber sheets was clearly visible since the CNF-modified epoxy resin appears black. Time-lapse images were created from the video recordings and compared against the ideal computer simulations. The point injection technique was used for injecting the mold with epoxies containing 0, 0.25, and 0.5 weight percents of CNF. The epoxies with 0.75 and 1.0 weight percent CNF were infused by the line injection method. This technique aids in the permeation of the fiber mats by the resin. Figure 18 shows the time-lapse imaging of the custom-made transparent mold injected with pure resin (0 weight percent CNF) using a point injection technique.

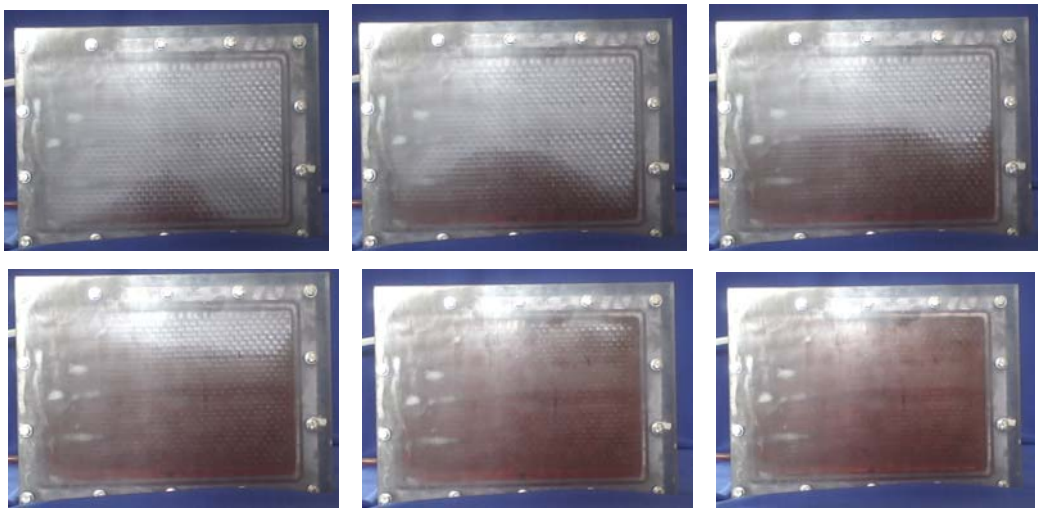

Figure 18: Time-lapse of mold injected with 0 weight percent CNF

Figure 19 shows the time-lapse imaging of the mold injected with 0.25 weight percent CNF-modified epoxy resin. Once again, a point injection technique was used. Likewise, Figure 20 shows the time-lapse of the mold injected with 0.5 weight percent CNF resin. Again, a point injection method was employed.

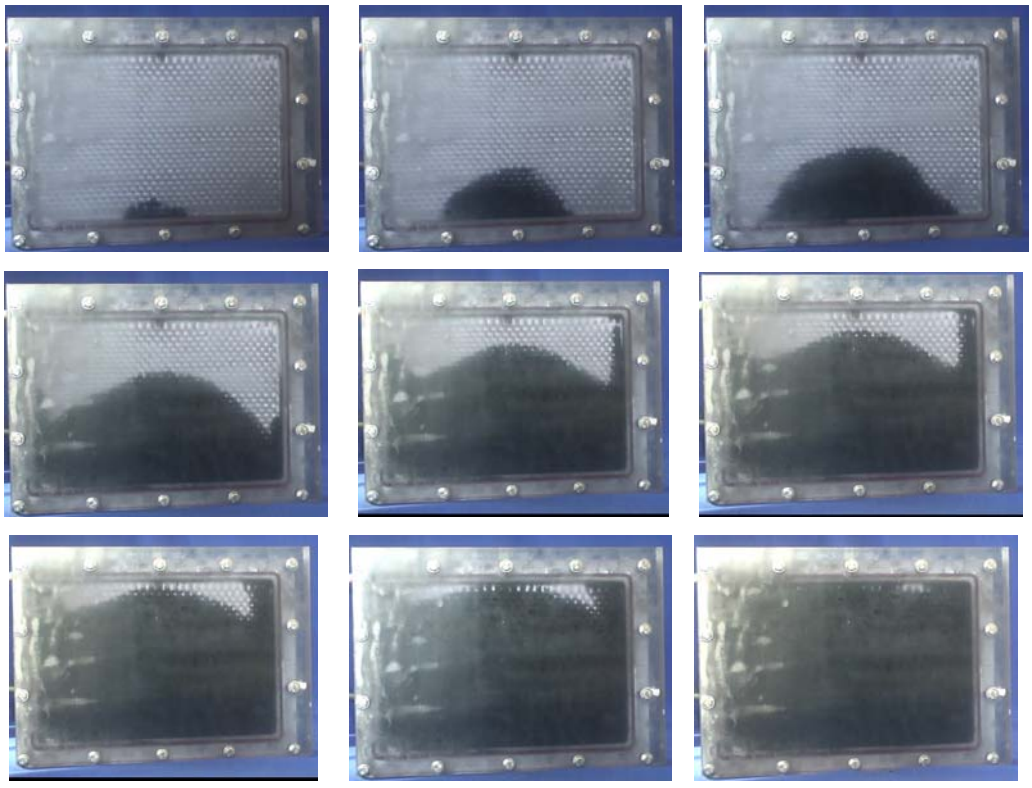

Figure 19: Time-lapse of mold injected with 0.25 weight percent CNF

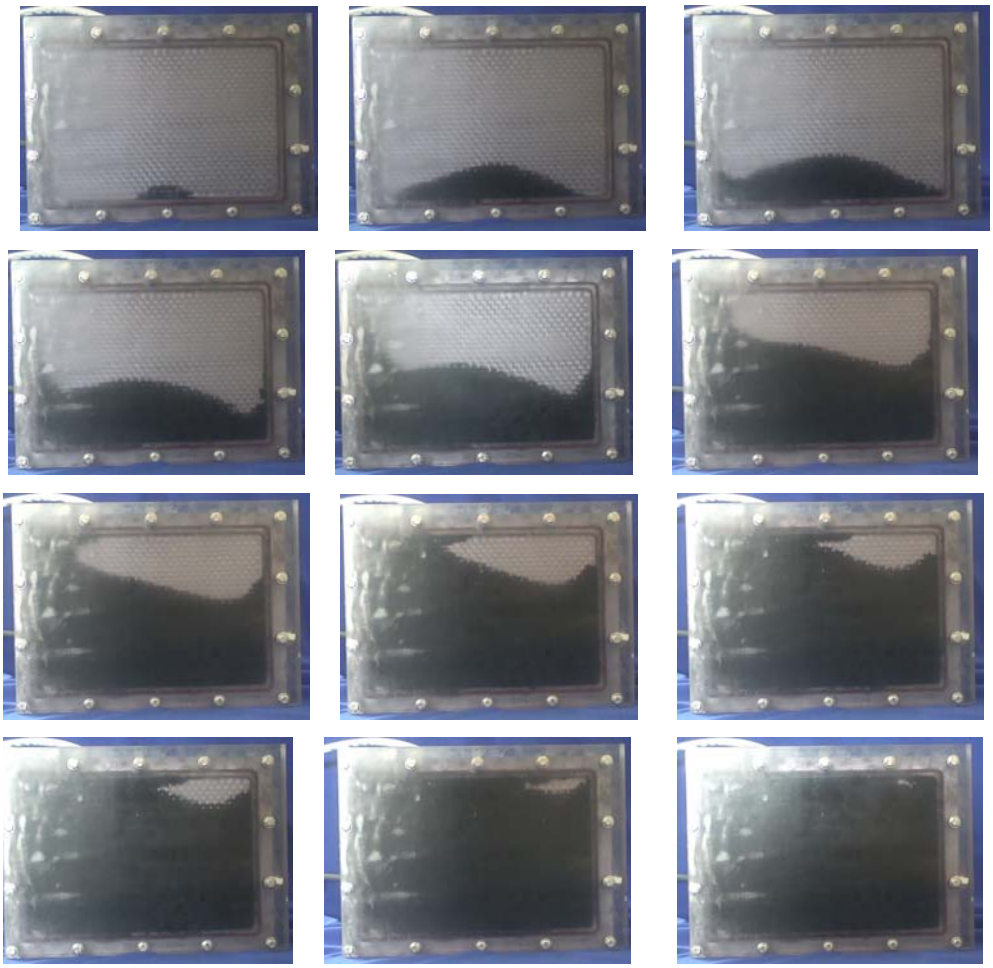

Figure 20: Time-lapse of mold injected with 0.5 weight percent CNF

For the remaining two resin samples, the line injection technique was used. Figure 21 shows the time-lapse imaging of the mold injected with 0.75 weight percent CNF resin and Figure 22 shows the mold injected with 1.0 weight percent CNF resin.

In general each of the five resin injections reflected their ideal simulations to some degree. The 0 and 0.25 weight percent CNF cases very closely matched their simulated counterparts. However, discrepancies arose in the latter 3 cases. Uneven rate of permeation is clearly seen in the 0.5, 0.75, and 1.0 weight percent injections. In the final case, the resin never completely permeated the glass fiber mat. This dry spot could have been stemmed from a number of different causes. Primarily, the dispersion of CNF

within the epoxy resin could have been too highly concentrated to successfully flow through the fiber mat. The flow of 1.0 weight percent CNF-modified resin may have actually been blocked within the fiber sheet. Also, insufficient pressure in an area may give rise to poor wetting and dry spots in this case. It can be seen in the simulation that the distributed pressure is at a low where this dry spot was formed.

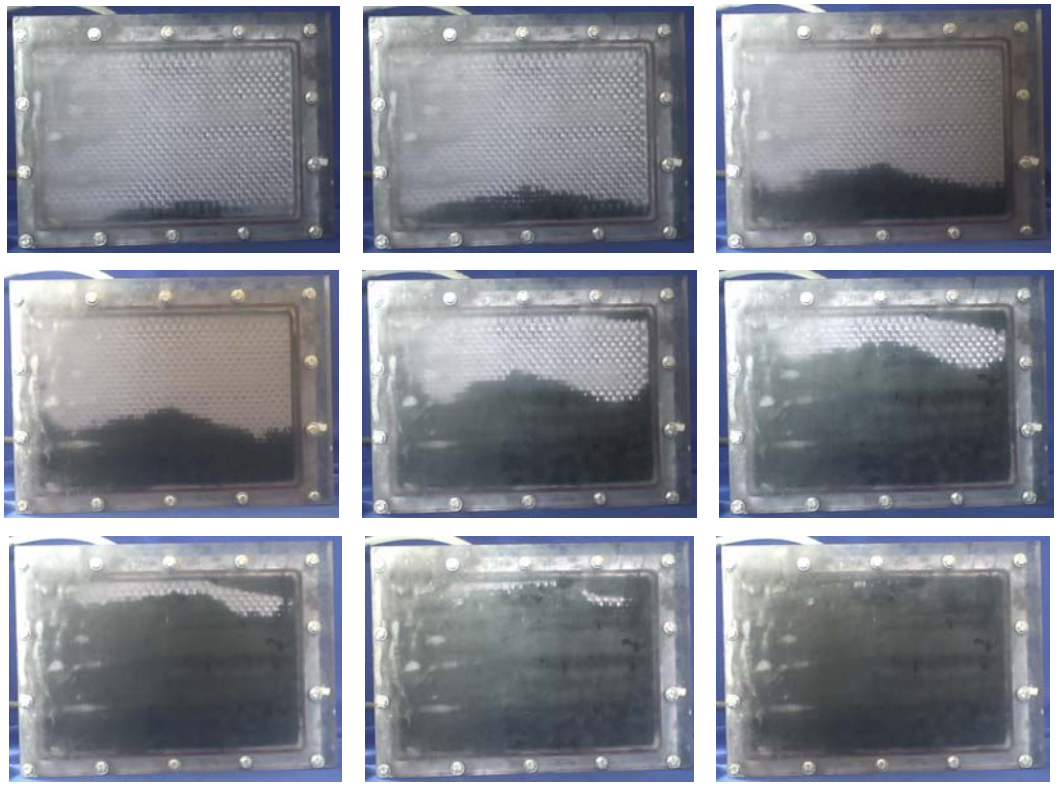

Figure 21: Time-lapse of mold injected with 0.75 weight percent CNF

Another possible source of inconsistencies in the resin flow comes from uneven layering of the glass fiber mats. Each of the mats are equal in thickness, but there is little that can be done to make sure that strands of fiber are not bunching up in some area, while spreading elsewhere. This may prove why the injected resin tends to fill one particular side of the fiber mat. In that same light, poor surface quality of the mold cavity and transparent lid could lend themselves to the same uneven filling.

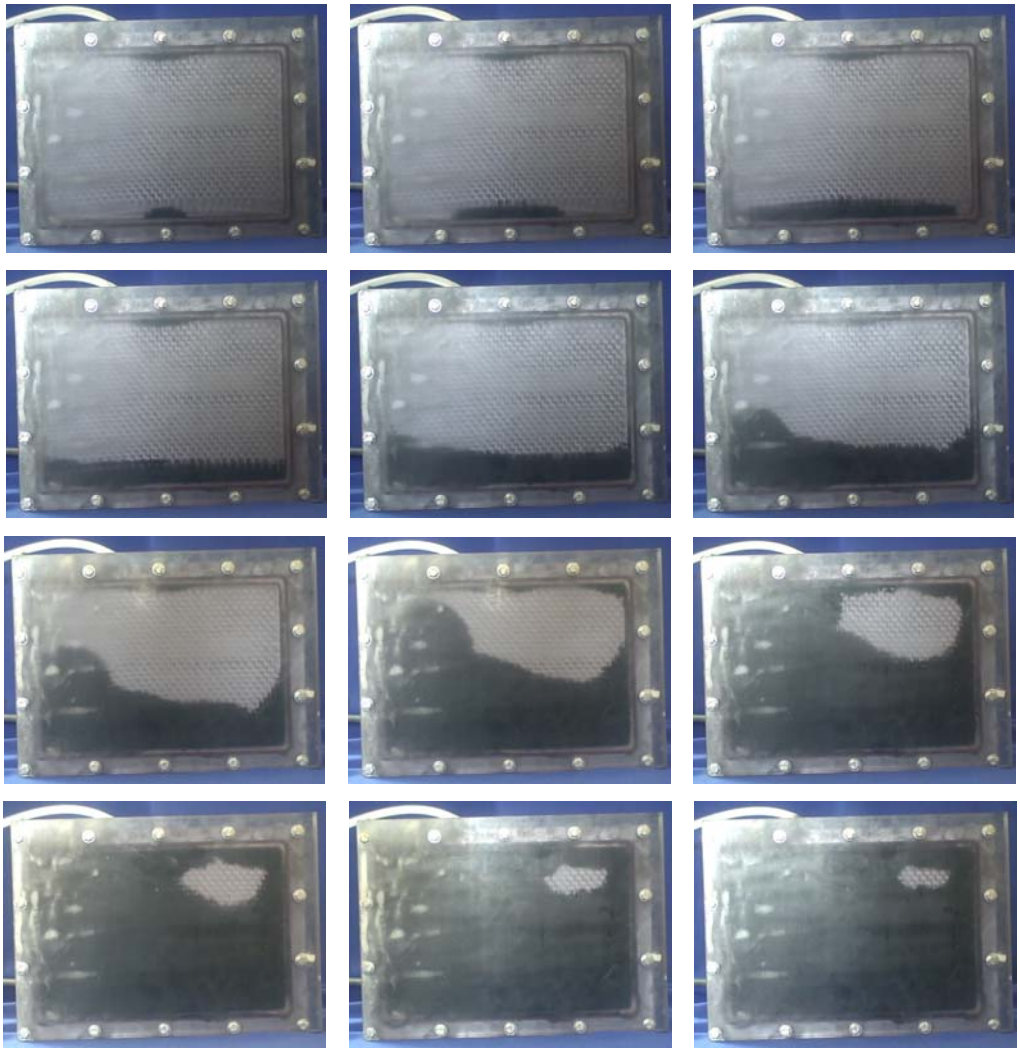

Figure 22: Time-lapse of mold injected with 1.0 weight percent CNF

One discrepancy affecting every one of the cases is edge effect. Resin flowing through the fiber mats does so much faster at the edge of the mold cavity. This is due to the ends of the glass fiber sheets being frayed; consisting of less fiber in that area. This effect can be decreased to a degree through very carefully cutting the fiber mats exactly to size or by inhibiting the flow at the corners of the mold cavity somehow. However, some edge effect will be present due to the woven fiber.

4.3 Damping

Scanning electron microscope (SEM) images were taken of each of the fabricated nanocomposite plates manufactured with the CNF-modified resin. The microstructure of the nanocomposite made with 1.0 weight percent CNF can be seen in Figure 23. The individual fibers of the carbon fiber mat can be seen stretching horizontally across the image, while dark areas of CNF-modified resin can be seen sporadically throughout. In much smaller concentrations, the carbon nanofibers are indicated by smaller light areas. The composite is essentially a multi-scale nanocomposite, since both the carbon fiber reinforced epoxy as well as the carbon nanofibers contribute to its damping properties.

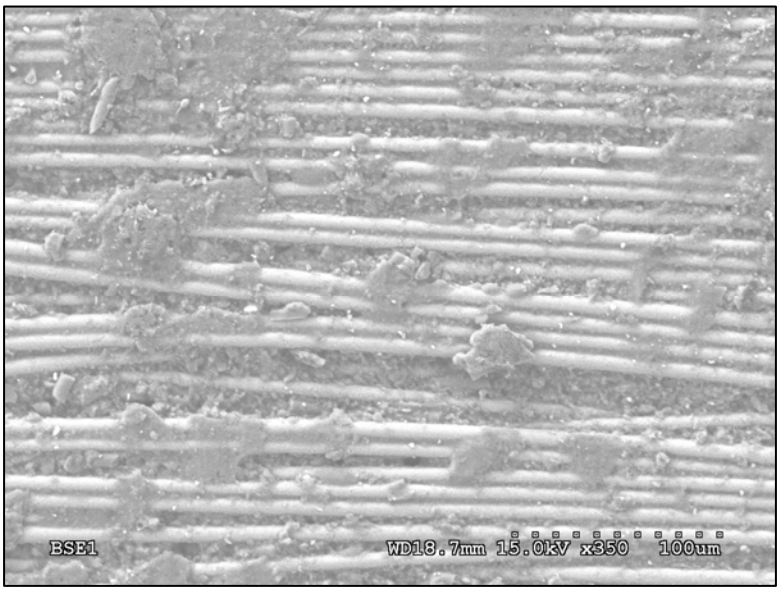

Figure 23: Microstructure of 1.0 weight percent CNF plate

4.3.1 Dynamic Mechanical Analysis

Four VARTM-formed nanocomposite plates were manufactured with epoxy resin containing different weight percentages of carbon nanofibers. Both the elastic modulus (storage modulus) and the viscous modulus (loss modulus) were obtained from the strain values recorded during the DMA testing process of each sample. The damping ratio was

then calculated from these modulus values by the elastic modulus by the viscous modulus. The plots of both the elastic modulus and viscous modulus with respect to temperature for each test sample can be seen in Figure 24a and Figure 24b, respectively.

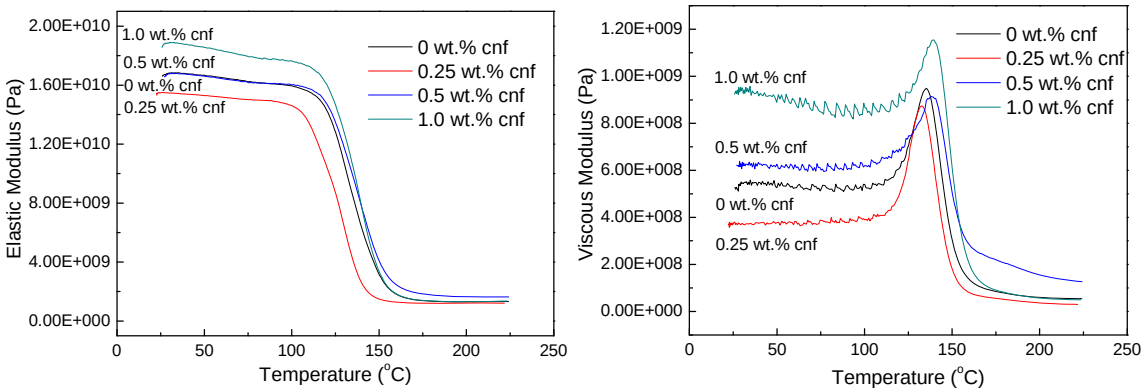

a) b)

Figure 24: Plots for a) Elastic modulus and b) viscous modulus

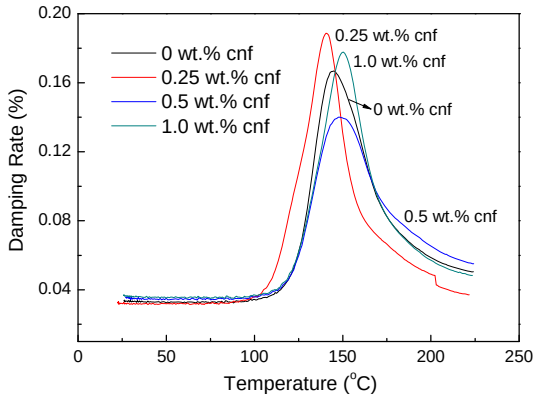

Figure 25: Damping ratio for each sample

The calculated damping ratios can be seen in Figure 25. In this graph the damping ratio was determined by reading the peak damping value for each sample. This peak occurs at the glass transition temperature. Although these damping ratios are not on the same scale as those previously discussed, the damping abilities of each sample can still be evaluated with relation to each other. It can be seen that the damping ratio of the 0.25 wt. % sample is higher than the rest, in spite of the conceived convention that

increased CNF content leads to better damping abilities. The 0.5 and 1.0 wt. % samples actually have worse damping abilities than the 0.25 wt. % sample. One reason for this is at higher CNF contents, poor dispersion in resins arises. Also, for the same reason, poor permeation of the fiber mats plays an integral role in inconsistent data. Even though the 0.25 wt. % sample contains less CNF content, the dispersion may be much more uniform.

4.3.2 Vibration Damping

The damping properties of four additional nanocomposite plates were determined by analyzing the vibration response to sweep sine excitations using piezoceramic patches. Each plate was tested with a sweep sine signal actuated at the center of the plate and sensed at the corner of the plate by a pair of PZT actuator sensors. A dSpace data acquisition (DAQ) system was used to record the nanocomposite plate's frequency response to the sweep sine excitation. The response of the nanocomposite plates were recorded in both time and frequency domains. The time domain response of the nanocomposite plates are presented in Figure 26. A direct comparison of time domain response is presented in Figure 27.

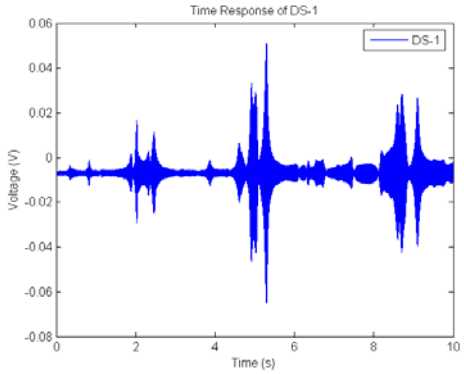

(a) DS-1

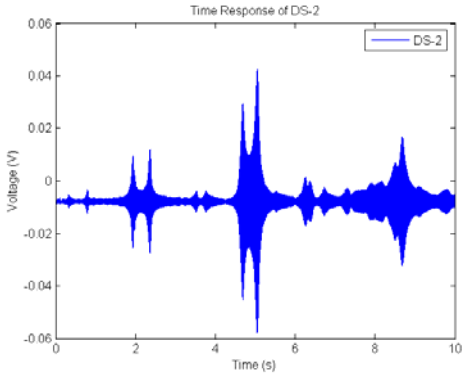

(b) DS-2

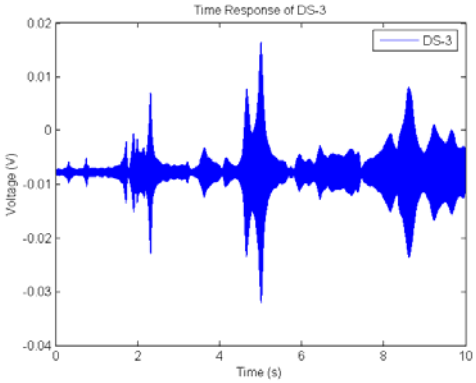

(c) DS-3

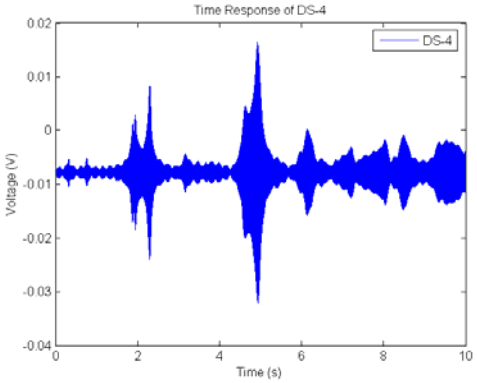

(d) DS-4

Figure 26: Time Domain Responses of Nanocomposite Plates

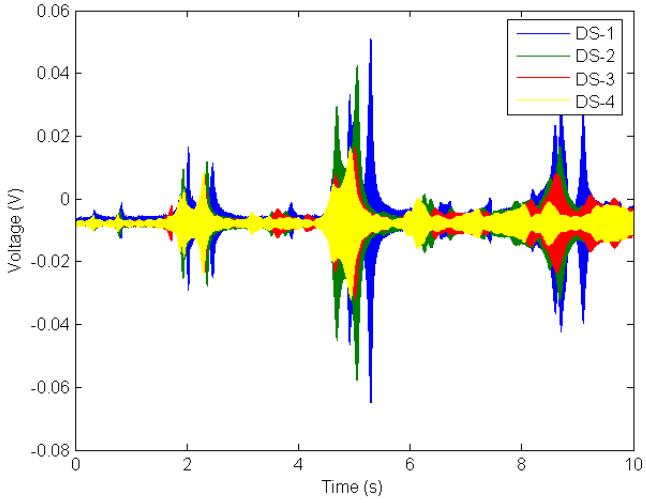

Figure 27: Direct Comparison of Time Domain Responses

The time based responses were insufficient to quantitatively determine the damping ratios of the nanocomposite plates and a frequency based analysis technique was adapted. The recorded data was processed by MatLab to produce a Bode plot of the nanocomposite plate's responses. The decibel magnitude of the plate's response was calculated through the conversion

$$\|V_{dB}\| = 10 \times 20 \log V \,, \tag{18}$$

where V is the voltage recorded by the dSpace software and V_{dB} is the magnitude of the response in decibels.

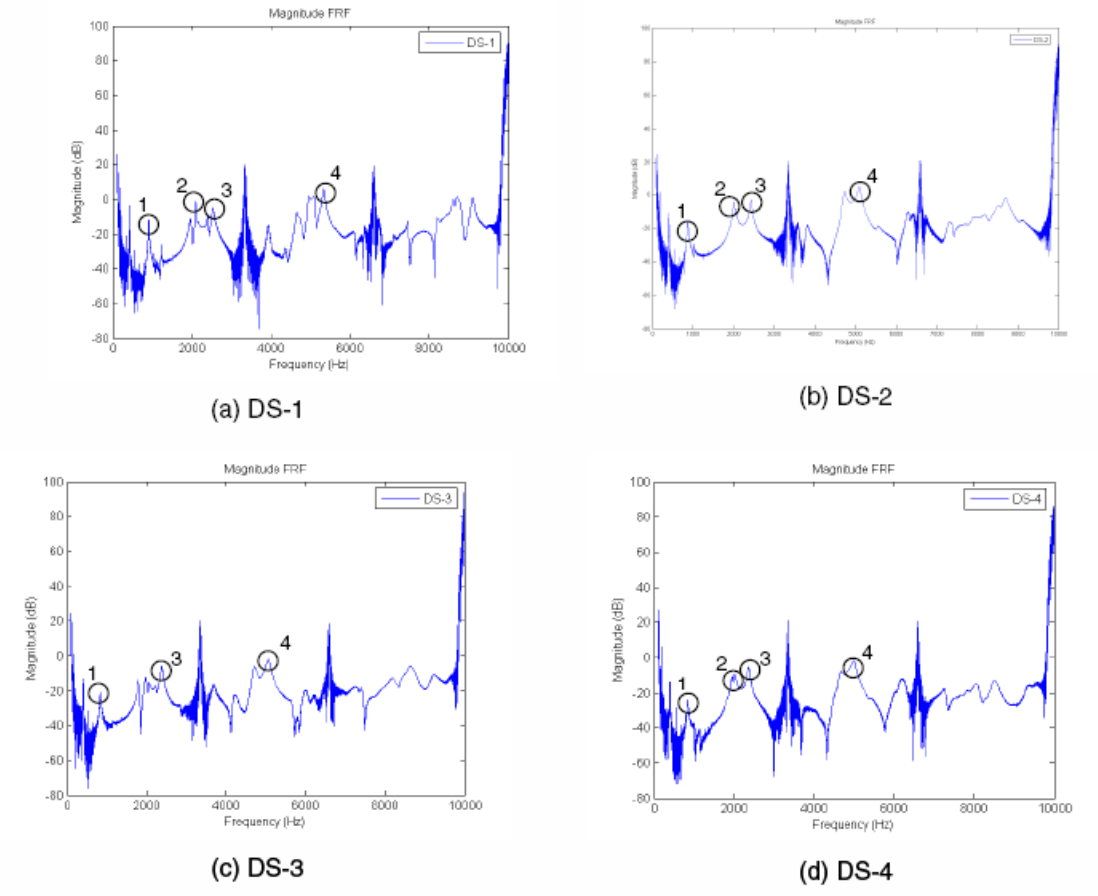

Figure 28: Frequency response of each sample with highlighted peaks

The magnitude was multiplied by 10 because the dSpace DAQ has a built-in gain of 0.1 for data input. Data for each nanocomposite plate was converted to decibel magnitude and plotted with respect to excitation frequency. The plots for the nanocomposite plates are presented in Figure 28. The magnitude plots have peaks in similar frequency ranges and share a similar shape. For analysis, the low frequency and high frequency ranges were ignored due to the noise introduced by the numerically determined transfer function.

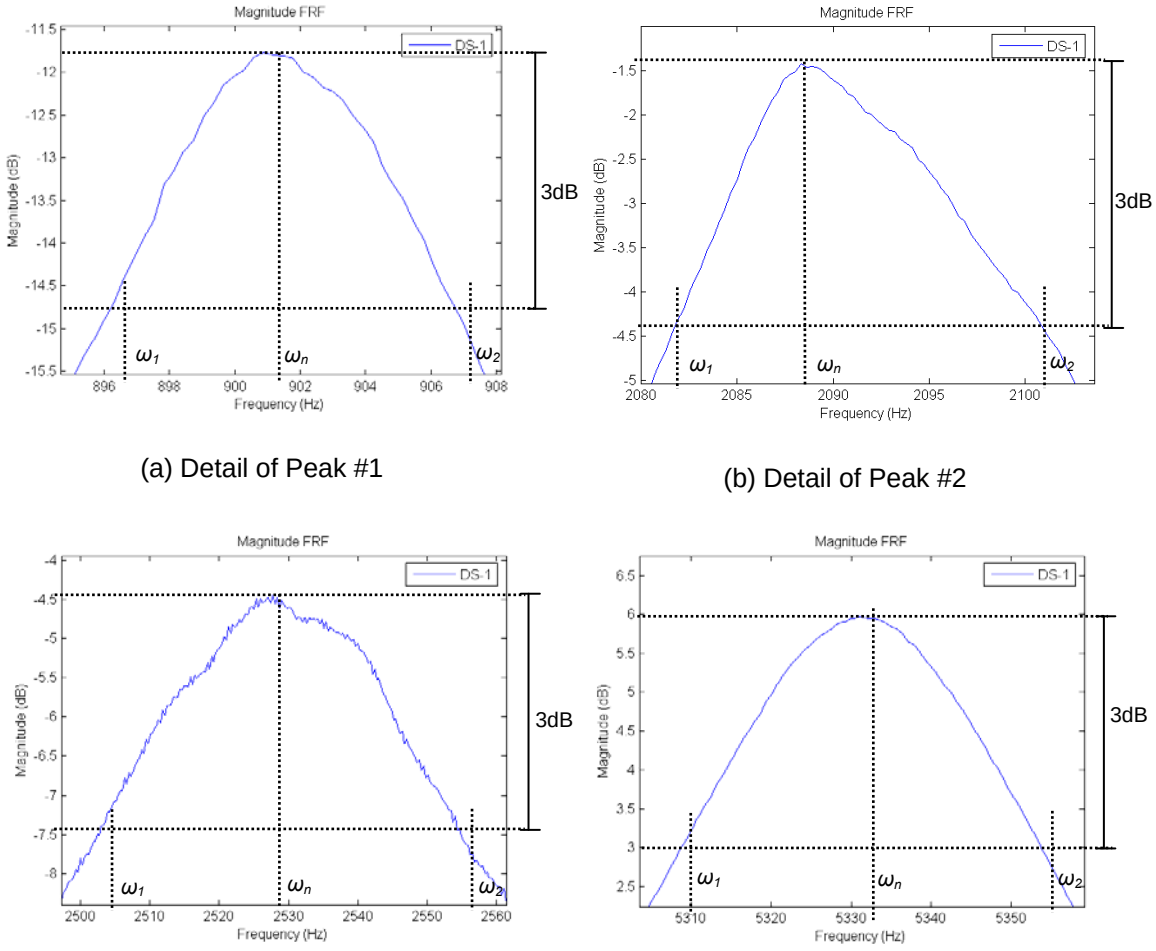

(a) Detail of Peak #1

(b) Detail of Peak #2

(c) Detail of Peak #3

(d) Detail of Peak #4

Figure 29: Details of Peaks for Sample DS-1

Four peaks in the frequency-based response were used to find the damping ratio for each of the nanocomposite plates. The peaks analyzed are identified in Figure 29. Enlarged details of the identified peaks used in analysis of plate DS-1 are provided in Figure 29 as an example of the analysis process in identifying the relevant frequencies. For each of the identified peaks, ω_n, ω_1, and ω_2 are identified. The relevant frequencies are summarized in Table 4. The frequencies for Peak #3 of sample DS-3 are not listed because the vibration at that frequency range was attenuated and the analysis of that peak was not possible.

Table 4: Summary of peak frequencies

	Peak #1 Frequencies (Hz)			Peak #2 Frequencies (Hz)			Peak #3 Frequencies (Hz)			Peak #4 Frequencies (Hz)		
Sample	ω_n	ω_1	ω_2	ω_n	ω_1	ω_2	ω_n	ω_1	ω_2	ω_n	ω_1	ω_2
DS-1	900.75	896	906.75	2088	2082	2101	2527	2503	2554	5332	5308	5354
DS-2	870	861	883	2003	1985	2025	2429	2406	2449	5092	5051	5124
DS-3	833	822	843	N/A	N/A	N/A	2387	2364	2407	5057	5009	5099
DS-4	838	826	860	2018	1997	2051	2367	2337	2395	4975	4911	5035

The frequencies noted for each of the identified peaks were analyzed using the half-band power algorithm to determine the damping ratio of the plate. The calculated damping ratios for each of the identified peaks and the averages for the sample are presented in Table 5. The damping ratios are represented graphically in Figure 30.

Table 5: Summary of damping ratios at peak responses for each sample

Sample	Peak #1	Peak #2	Peak #3	Peak #4	Average
DS-1	0.0060	0.0045	0.0101	0.0043	**0.0062**
DS-2	0.0126	0.0100	0.0089	0.0072	**0.0097**
DS-3	0.0126	-	0.0090	0.0089	**0.0102**
DS-4	0.0202	0.0134	0.0123	0.0125	**0.0146**

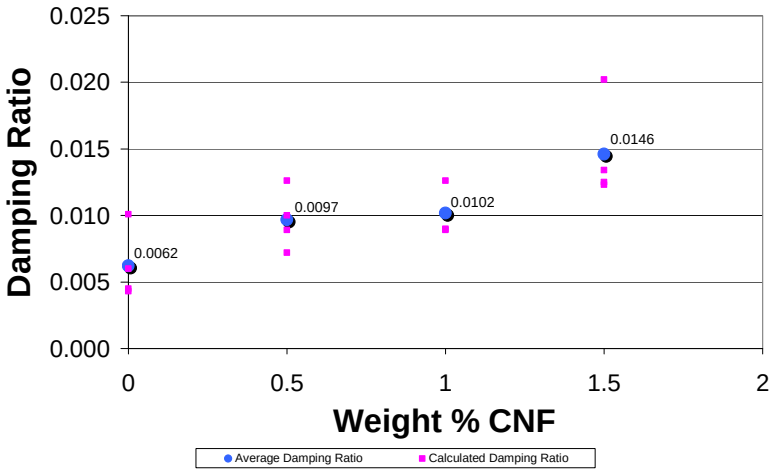

Figure 30: Plot of damping ratios vs. weight % CNF

From Figure 30, it can be seen that as the weight percentage of carbon nanofiber (CNF) increases in the samples, so too does the damping ratio of the nanocomposite. For a 1.5 weight percentage increase of CNF, there was an observed gain of 2.35 in the damping ratio. This increase in damping ratio can be qualitatively observed in Figure 27, where the amplitude of the responses decreased with increase of CNF weight percentage even though the peaks appear at relatively the same times in the response. It can be seen that there is a significant decrease in vibration amplitude between sample DS-1, which had the least weight percentage of CNF, and DS-4, which had the greatest weight percentage of CNF. The decrease of damping ratio with increase of weight percentage CNF is further qualitatively supported by the broadening of peaks in the magnitude plots in the frequency domain. For peaks at similar frequency ranges, the shape of the peak flattens as the weight percentage of CNF increases, resulting in smaller peak amplitudes indicative of increasing damping ratios.

The damping tests were also conducted on the composite laminates containing a carbon nanopaper sheet as a surface layer. During the damping test, the sweep sinusoidal signals were used as excitation source for the PZT actuator to get the frequency response of the system. Two sweep sine signals were used for the test. One sweep sine was from 100Hz to 2000Hz to get detailed information about the first mode frequency. The other sweep sine was from 100Hz to 10,000Hz to excite the first few modes. The sweeping period of both signals were set to 20 seconds. The sampling frequency was set to 40k Hz. For the nanocomposite plate with carbon nanopaper sheet as surface layer, the time domain responses of both sweep sine excitations are shown in Figure 31a and Figure 31b, respectively. The peak value in the sweep sine response represents resonance at a certain natural frequency. From the sweep sine responses, it can be clearly seen that the peak of first, second, and third modes are significantly reduced for the nanocomposite plate, which indicates its improved damping ability.

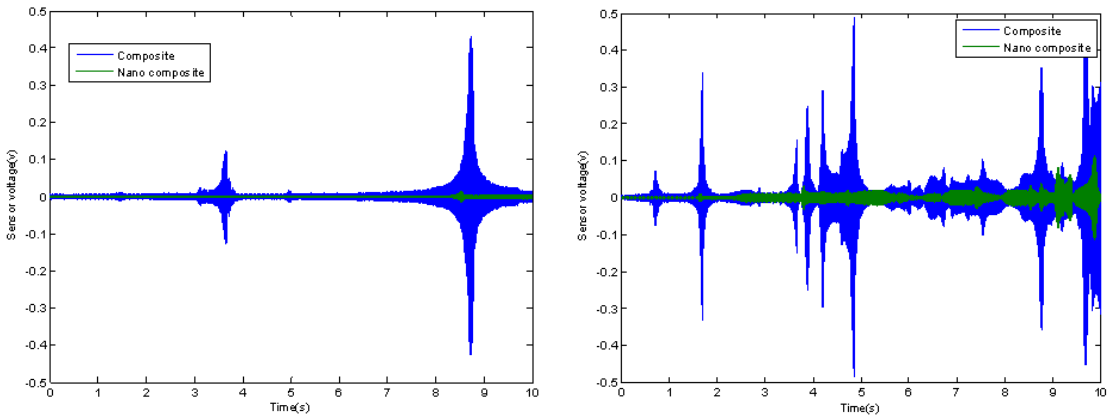

a) 100 – 2000 Hz b) 100 – 10,000 Hz

Figure 31: Time domain response of plate with and without CNF paper

To further demonstrate the improved damping for the nanocomposite plate, the frequency response of the regular composite plate and a nanocomposite plate were compared. The identical sweep sine excitation signals were used, and can be seen in Figure 32a and Figure 32b.

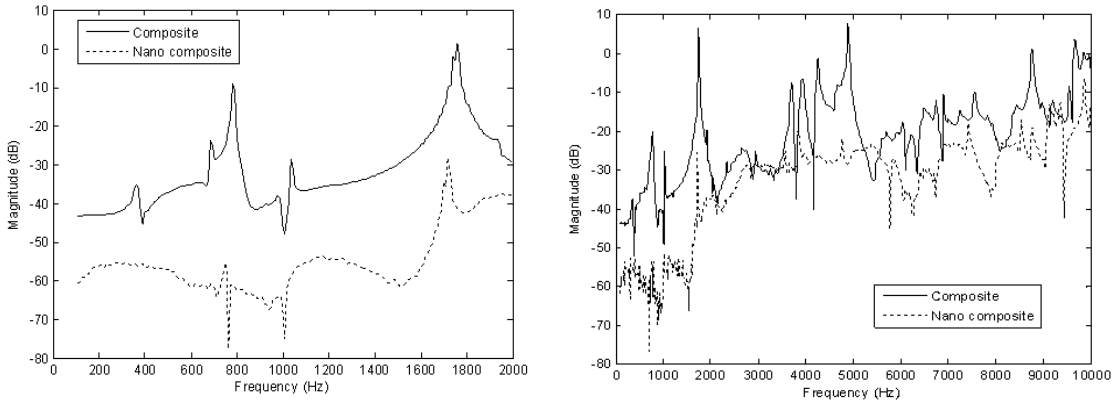

a) 100 – 2000 Hz b) 100 – 10,000 Hz

Figure 32: Frequency domain response of plate with and without CNF paper

From these images, it can be seen that the peak magnitude of the first three modes had dropped dramatically. This means the damping ratio values of the nanocomposite plate at these natural frequencies are much larger than those of the regular composite plate. The difference in magnitude for each of the three modes is organized in Table 6.

Table 6: Frequency domain response effect of CNF paper on the first three modes

	1st mode (dB)	2nd mode (dB)	3rd mode (dB)
Peak value (Standard composite)	-20.30	6.12	-7.65
Peak value (Nanocomposite)	-53.30	-25.67	-25.35
Drop value	**33.00**	**31.79**	**17.70**

4.3.3 Acoustic Damping

The same CNF paper-laden nanocomposite plates were tested for their acoustic damping properties. The plates were actuated with a PZT patch, while a sound level meter was used to record the acoustic response. The decibel response with respect to time can be seen in

Figure 33. The response of the first two modes have been enlarged to more clearly see the difference between standard composite and nanocomposite.

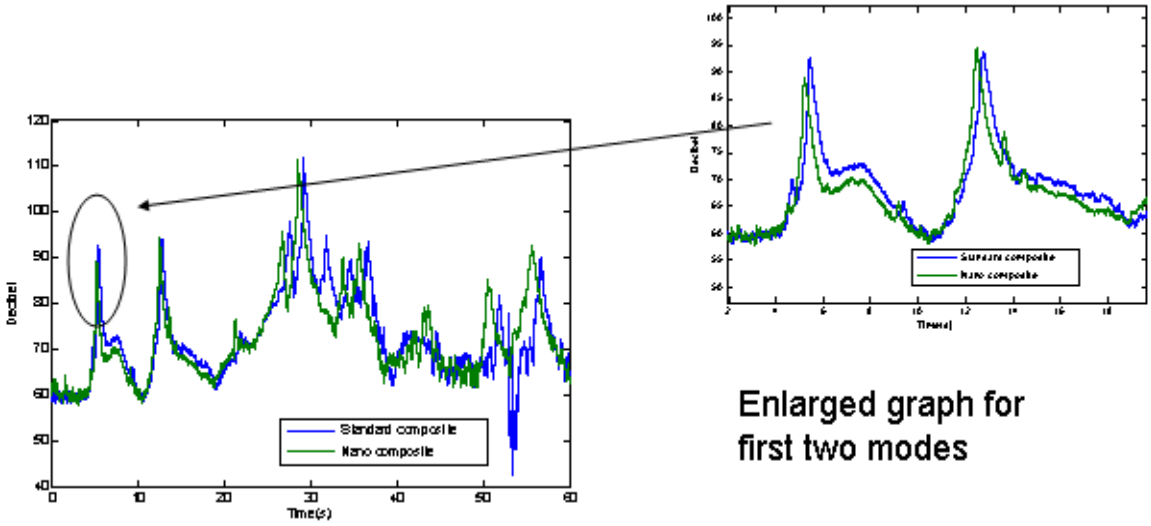

Figure 33: Time-domain decibel response with enlarged first two modes

The excitation source was once again a sweep sine signal. This signal ranged from 80 to 8,000 Hz in 60 seconds. It is shown in the enlarged view that the acoustic response in the first two modes has indeed been damped for the nanocomposite plate.

In the acoustic response, the increased damping effect of the nanocomposite is much less apparent than in the vibrational response. The retrieved data may include much noise from a couple of sources. One source of noisy data comes from the fact that the acoustic meter and test plate are in an open system where the surrounding

environment undoubtedly interferes with the retrieved data. The testing apparatus for the acoustic vibration including the sound lever meter can be seen in Figure 34.

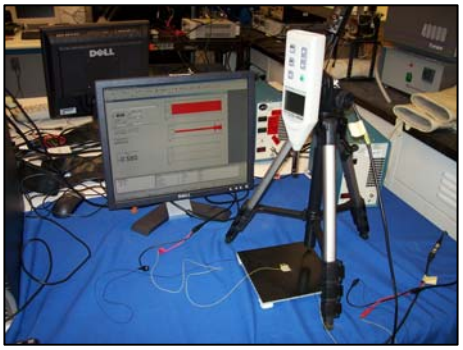

Figure 34: Acoustic vibration testing apparatus

Another important factor to note is that test plate was resting on a table, which would have damped some of the plates vibrations and possibly introduce others. For retrieving more accurate data, the test plate should be suspended off of any surface that may transmit vibrations. Also, the entire testing apparatus should be enclosed within a closed system to aid in filtering out undesired noise.

CHAPTER 5.

CONCLUSIONS

5.1 Isothermal Curing Analysis

Differential scanning calorimetry (thermal-based) and rheological (viscosity-based) analyses were conducted in order to characterize the curing behavior of CNF-modified polymer resin. The data generated from the DSC measurements provided the heat generated by the resin samples throughout the curing process. Its degree of cure was calculated from this data. A logarithmic plot showed the curing process being activated within the first 10 minutes for each sample. After which, the reaction slowed down. It was apparent that curing CNF-resin at lower temperatures achieved a higher degree of cure faster than at higher temperatures.

A series of rheological experiments were conducted in order to illustrate a trend in gel times with respect to curing temperature and resin CNF content. The resin's viscosity was recorded throughout its isothermal curing reaction with a viscometer. It was found that each resin sample at room temperature possessed a distinct viscosity value that generally increased with respect to CNF content.

After initially heating the resin to begin the curing process, the viscosities fell drastically for each sample. The pure resin actually reached a viscosity of 0 cP. As the CNF content increased in the resin, the minimum viscosity also increased. The viscosity of the 1.0 weight percent CNF-resin never fell below 630 cP, which causes potentially serious flow and permeability issue in closed mold injection. CNF-epoxy resin at this viscosity may lead to dry spots or voids within the fabricated nanocomposite.

In the final phase of the resin's curing, its viscosities increased exponentially. It was found that the curing time decreased with the addition of CNF content in the resin. The discrepancies that exist in these rheological trends were likely due to improper CNF dispersion or disturbances in the isothermal curing process.

5.2 Flow Visualization Analysis

The process analysis of mold filling and pressure distribution was conducted using Control Volume Finite Element Method. The mold filling simulation was validated with flow visualization in a transparent mold. Two types of mold injections were considered, point injection and line injection.

In general, each of the five resin injections reflected their ideal simulations. The 0 and 0.25 weight percent CNF-modified resins very closely matched their simulated counterparts. However, the latter three cases diverged from the ideal results. Uneven rate of permeation was clearly observed in the 0.5, 0.75, and 1.0 CNF-resin injections. In the highest concentration of CNF, the resin never completely permeated the fiber mat. This dry spot may have been caused by insufficient injection pressure, poor surface quality of the mold cavity, uneven layering of the fiber mats, or uneven dispersion of CNF within the epoxy resin.

The most apparent discrepancy affecting every the case was edge effect. Resin flowed through the fiber mats much faster at the edge of the mold cavity, due to the frayed ends of the glass fiber mats. This effect, along with increased CNF content, has the potential for inhibiting the complete permeation of the resin through the fiber.

5.3 Damping Analysis

Damping analysis was conducted on both nanocomposites containing CNF-modified epoxy resin and nanocomposites containing a sheet of CNF paper. For each case, multiple test plates were fabricated using Vacuum-Assisted Resin Transfer Molding process. They were tested with both DMA analysis, and with piezoceramic actuators and sensors to determine the effect of CNF on the damping ratio of the plates. A sweep sine excitation signal was used to actuate a PZT patch on the surface to vibrate the plate. The response was detected by a second PZT patch bonded to the surface. The response was analyzed by half-power algorithm to determine the damping ratio of the plates.

For the testing conducted on the nanocomposites with CNF-modified epoxy resin, the results also showed that as the weight percentage of CNF in the paper increased, the damping ratio of the plates increased.

From the DMA analysis, it was concluded that the damping ratio of the 0.25 weight percent CNF sample was higher than that of the other samples regardless of increased CNF content. At higher CNF concentrations, poor CNF dispersion and the resulting flow inhibition becomes a predominant factor in VARTM-formed nanocomposites. Even though the 0.25 weight percent sample contained less CNF content, the dispersion may have been much more uniform, which guaranteed that the beneficial damping effects were distributed throughout the entire plate.

From the PZT-patch analysis, the results confirmed that as the weight percentage of CNF increased in the nanocomposite plates, so too does the damping ratio of the plate. For a 1.5 weight percentage increase of CNF, there was an observed gain of 2.35 in the damping ratio. This trend was further qualitatively supported by the broadening of the

peaks in magnitude in the Bode plots. For peaks at similar frequency ranges, the shape of the peak flattened as the weight percentage of CNF increased, resulting in smaller peak amplitudes indicative of increasing damping ratios.

For the testing conducted on the nanocomposites with an embedded layer of CNF paper on the surface, the results also showed that as the weight percentage of CNF in the paper increased, the damping ratio of the plates increased. The tests also indicated significant increase of the damping ratios at higher frequencies and slight change in stiffness of composite laminates due to the incorporation of carbon nanopaper sheet. Even though the results from the acoustic tests were not as conclusive, they still supported the beneficial effects of CNF obtained by DMA and PZT testing.

Both of these conclusions indicated that the addition of CNF to standard composites reduced the vibration of the composite to cyclical excitation. The nanocomposites are essentially multi-scale nanocomposites, where both the carbon fiber reinforced epoxy as well as the carbon nanofibers contribute to its damping properties. More importantly, the results suggest that to achieve an increase in damping, CNF does not need to be homogenously dispersed throughout the composite matrix. Since the CNF was introduced as a sheet in the VARTM process, the results indicate that this manufacturing process is viable to create low cost, easily manufactured nanocomposites with significant damping advantages over traditional composites.

5.4 Future Research Directions

There are a few notable and potentially rewarding directions for which the future research in damping effectiveness may take. Currently, testing was conducted for two distinct types of nanocomposites. One type containing CNF paper and the other type

containing dispersed nanofibers within its polymer resin matrix. Research and testing should be conducted for nanocomposites containing both CNF paper as well as dispersed nanofibers within the polymer matrix. This combined technique may result in even more favorable results.

With respect to using CNF paper along with traditional carbon fiber reinforced polymer laminates, only one single surface layer of CNF paper at a time has been added for improving damping performance. The effect of the CNF paper should be examined by placing it within the layers of the composite laminate. The effects of placing multiple interlaminar layers of CNF paper between the composite laminate should also be studied.

Currently, both the CNF paper and CNF-modified epoxy resin contain randomly dispersed carbon nanofibers. Though the omni-directional arrangements of nanofibers are beneficial to improving damping properties, the alignment of nanofibers in both the CNF paper and the composite matrix should be researched. With the ability to align nanofibers in a desired direction, the opportunity for applications involving magnetic or electrical conduction opens up.

Lastly, better dispersion techniques for nanofibers within nanocomposites need to be developed, especially when injecting resin at higher weight percents of CNF. The obstacle of poor CNF dispersion needs to be overcome if the VARTM process is to continue being used for the manufacturing of nanocomposites. For injecting a polymer, such as CNF-modified epoxy resin, that contains high weight percents of nanofibers, some processing variables need to be adjusted. Possible adjustments may be made to the injection temperature, injection pressure, mold temperature, nanofiber pre-mix dispersion, or nanofiber pre-injection treatment.

LIST OF REFERENCES

Advani, S. G., Flow and Rheology in Polymeric Composites Manufacturing, *Elsevier Publisher*, 1994.

Ajayan, P.M., J. Suhr, and N. Koratkar. Utilizing Interfaces in Carbon Nanotube Reinforced Polymer Composites for Structural Damping, *Journal of Material Science*, Vol. 41, 2006, pp. 7624-7829.

Breuer, O. and Uttandaraman S. Big Returns from Small Fibers: A Review of Polymer/Carbon Nanotube Composites, *Polymer Composites*, 2004, Vol 25, No. 6, pp. 631-645.

Chang, Christiana. *Determination of Damping Ratio in Nanocomposite Plates Using Piezoceramics*. University of Houston.

Gonis, J., Simon, G. P., and Cook, W. D., Cure Properties of Epoxies With Varying Chain Length as Studied by DSC. *Journal of Applied Polymer Science*, 1999.

Gou, J., O'Brient, S., and Gu, H., and Song, G. Damping Augmentation of Nanocomposites Using Carbon Nanofiber Paper. *Journal of Nanomaterials*, 2006.

Gou, J., Zhang, C., Liang, Z., Wang, B., and Simpson, J. Resin Transfer Molding Process Optimization Using Numerical Simulation and Design of Experiments Approach.. *Polymer Composites*, 2003.

Gou, J., Zhao, Z., Ji, X., Sumerlin, H., and Song, G. *Structural Damping Enhancement of Fiber reinforced Composites via Carbon Nanopaper Sheets*. University of South Alabama, University of Houston.

Grenier-Loustalot, M. F. and Grenier, P., The Mechanism of Epoxy-resin Curing in the Presence of Glass and Carbon Fibers. *Polymer*, 33, 1187. 1992.

Finegan, I. and Gibson, R., Recent Research on Enhancement of Damping in Polymer Composites. *Composite Structures*, 44 (1999) 89-98.

Hatakeyama, T. and Quinn, F. X., *Thermal Analysis Fundamentals and Applications to Polymer Science*. John Wiley & Sons, 1994.

Hinrichs, R. J. Rheological Cure Transformation Diagrams for Evaluating Polymer Cure Dynamics in Chemorhology of Thermosetting Polymers. May, C. A., *ACS Symposium Series*, 227, American Chemical Society, Washington, D. C., 187, 1983.

Horr, A. M. and Schmidt, L. C., Modelling of Nonlinear Damping Characteristics of a Viscoelastic Structural Damper. *Engineering Structures*, vol. 18, pp. 154-161, 1996.

Koratkar, N., Wei, B., and Ajayan, P., Carbon Nanotube Films for Damping Applications. *Advanced Materials*, 2002, 14, No. 13-14.

Li, W. Process Analysis and Adaptive Control of Resin Transfer Molding. *dissertation*, University of Alabama, 2001.

Mallick, P. K., *Fiber-Reinforced Composites: Materials, Manufacturing, and Design, Third Edition*. CRC Press, Boca Raton, 2008.

Scientific American. *Key Technologies of the 21st Century*, New York: W.H. Freeman and Company, 1996.

Song, G., *Acoustic Test and Vibration Test of Nano Composites*. Department of Mechanical Engineering University of Houston.

Suhr, J. and Koratkar, N., Energy Dissipation in Carbon Nanotube Composites: A Review. *Journal of Materials Science*, 43: 4370-4382, 2008.

Sun, Liangfeng., Thermal Rhological Analysis of Cure Process of Epoxy Prepreg. *dissertation*. Louisiana State University, 2002.

Tanaka, Y. and Bauer, R. S., *Curing Reaction: Epoxy Resins Chemistry and Technology, Second Edition*. Marcel Dekker, Inc., New York, 285, 1988.

Xu, L. and Schlup, J. R., Etherification Versus Amine Addition During Epoxy Resin/Amine Cure: An In Situ Study Using Near-Infrared Spectroscopy. *Journal of Applied Polymer Science*, 67, 895, 1998.

Yang, F., Yao, K. D., and Koh, W., Kinetics Analysis of the Curing Reaction of Fast Cure Epoxy Prepregs. *Journal of Applied Polymer Science*, 73, 1501, 1999.